Transnational University Limburg is a unique collaboration of two universities in two countries: the University of Hasselt and Maastricht University.

UHASSELT
KNOWLEDGE IN ACTION

www.uhasselt.be
Universiteit Hasselt
Campus Hasselt:
Martelarenlaan 42 | 3500 Hasselt
Campus Diepenbeek:
Agoralaan Gebouw D | 3590 Diepenbeek

UHASSELT
KNOWLEDGE IN ACTION

Maastricht University

Faculty of Medicine and Life Sciences
School for Life Sciences
Master of Biomedical Sciences

Master's thesis

Cholesterol in macrophage-derived extracellular vesicles drives remyelination in the brain

Jeroen Guns

Thesis presented in fulfillment of the requirements for the degree of Master of Biomedical Sciences, specialization Molecular Mechanisms in Health and Disease

SUPERVISOR :
Prof. dr. Jeroen BOGIE

MENTOR :
De heer Sam VANHERLE

2021
2022

UHASSELT
KNOWLEDGE IN ACTION

Maastricht University

Faculty of Medicine and Life Sciences
School for Life Sciences
Master of Biomedical Sciences

Master's thesis

Cholesterol in macrophage-derived extracellular vesicles drives remyelination in the brain

Jeroen Guns

Thesis presented in fulfillment of the requirements for the degree of Master of Biomedical Sciences, specialization Molecular Mechanisms in Health and Disease

SUPERVISOR :

Prof. dr. Jeroen BOGIE

MENTOR :

De heer Sam VANHERLE

Cholesterol in macrophage-derived extracellular vesicles drives remyelination in the brain*

Guns J[1], Vanherle S[1], and Bogie J[1]

[1]Immunology and Infection, Biomedical Research Institute, Universiteit Hasselt, Campus Diepenbeek, Agoralaan Building C - B-3590 Diepenbeek

*Running title: *Cholesterol controls remyelination*

To whom correspondence should be addressed: Prof. dr. Jeroen Bogie, Tel: +32 (11) 26 92 61; Email: jeroen.bogie@uhasselt.be

Keywords: Multiple sclerosis, macrophages, extracellular vesicles, cholesterol, remyelination

ABSTRACT

Failure of remyelination underlies the progressive nature of demyelinating diseases, such as multiple sclerosis (MS), which is a devastating autoimmune disease affecting the central nervous system (CNS). Macrophages are abundantly present in active MS lesions and play a pivotal role in disease progression and resolution. To date, however, it remains largely unknown how macrophages contribute to CNS repair. Here we demonstrate that extracellular vesicles (EVs) released by macrophages with a repair-promoting phenotype promote oligodendrocyte progenitor cell (OPC) maturation *in vitro,* and enhance remyelination in an *ex vivo* cerebellar brain slice and the *in vivo* cuprizone model. Furthermore, we demonstrate that the pro-regenerative impact of repair-associated macrophage-derived EVs is attributed to increased cholesterol levels present in these EVs, but does not rely on increased activation of the cholesterol-sensing liver X receptors in OPCs. Collectively, our results highlight that EV-associated cholesterol is a key determinant of the regenerative properties of EVs released by lesional macrophages, thereby highlighting the diagnostic and therapeutic potential of EVs in MS and other demyelinating diseases.

INTRODUCTION

Demyelinating diseases, such as multiple sclerosis (MS), are characterized by loss of the protective myelin sheath and neurodegeneration, often accompanied by overt neuroinflammation (1, 2). Progressive demyelination, axonal damage, and neuronal loss, which are initiated by an autoimmune response developed against CNS-derived antigens, are typical for MS (3, 4). A major pathological hallmark of the disease is the accumulation of peripheral- and CNS-derived macrophage subsets within the CNS lesions (5, 6). For a long time, it was thought that macrophages solely acquire a disease-promoting phenotype. More specifically, disease-associated macrophages (DAMs) promote neuroinflammation and neurodegenerative events by releasing inflammatory mediators and stimulating leukocyte activity and infiltration into the CNS (7, 8). However, we and others recently found that macrophages can also acquire a protective functional phenotype, which suppresses neuroinflammation and enhances CNS repair (9-11). Disease-resolving effector functions of these repair-associated macrophages (RAMs) are the release of neurotrophic factors and clearance of inhibitory myelin debris (10, 12, 13).

Early in the disease course, endogenous repair processes are apparent as oligodendrocyte progenitor cells (OPCs) migrate to the lesion site and differentiate into mature, myelinating oligodendrocytes (14-16). However, with MS disease progression, these endogenous repair mechanisms frequently fail, resulting in chronically demyelinated axons (17-19). Several studies indicate that impairment of OPC maturation is largely responsible for this remyelination failure (20-22). To date, however, the mechanisms that underlie perturbed OPC maturation remain poorly understood.

Few studies indicate that the secretome of RAMs promotes the differentiation process of OPCs. For instance, IL-4 stimulated macrophage subsets promote remyelination through the release

of the neurotrophic factor activin A (23). Additionally, it was recently demonstrated that extracellular vesicles (EVs) derived from repair-associated microglia have a crucial role in driving the differentiation of OPCs into mature oligodendrocytes. In contrast, EVs secreted by disease-associated microglia appear to prevent remyelination (24). In support of the latter study, the role of EVs has gained significant interest as they seem to play a crucial role in intercellular signaling in many physiological and pathological processes (25). EVs are nanosized particles surrounded by a lipid bilayer membrane able to transport diverse biologically active molecules, such as proteins, nucleic acids, and lipids, from donor cells to neighboring and distant recipient cells. By doing so, they markedly affect recipient cell physiology (26, 27). To date, it remains unclear how macrophages contribute to endogenous repair processes and to which extent EVs are involved in the intercellular communication between macrophages and OPCs, thereby activating molecular pathways that promote CNS repair during MS. We hypothesize that EVs derived from RAMs promote OPC maturation and consequently enhance remyelination in different experimental set-ups. Identifying the molecular mechanisms that promote remyelination is essential for our understanding of CNS regeneration in demyelinating diseases such as MS, and to develop potential therapies to treat these diseases.

Here we report that EVs produced by RAM-like IL-4-stimulated bone marrow-derived macrophages (BMDMs) promote OPC differentiation *in vitro* and enhance remyelination in *ex vivo* and *in vivo* models mimicking remyelination. These beneficial effects are orchestrated by elevated cholesterol levels present in these EVs. Furthermore, we demonstrate that depleting cholesterol from IL-4-BMDM-derived EVs impairs remyelination, while replenishing cholesterol in DAM-like LPS-stimulated BMDM-derived EVs promotes CNS repair processes. The reparative impact of EVs released by RAMs did not rely on increased activation of liver X receptor (LXR), a nuclear cholesterol-sensing receptor that plays a key role in remyelination. Our findings highlight the importance of cholesterol present in macrophage-derived EVs in driving remyelination in the brain, which can be the basis for novel therapies to treat MS and other demyelinating diseases.

EXPERIMENTAL PROCEDURES

Animals – Wild-type (WT) C57BL/6J mice were purchased from Envigo. Mice were housed on a 12 h light/dark cycle with *ad libitum* access to water and standard chow diet or specific formulations as indicated. All animal procedures were conducted in accordance with the institutional guidelines and approved by the Ethical Committee for Animal Experiments of Hasselt University.

EV production, isolation, and purification – Bone marrow-derived macrophages (BMDMs) were isolated from femoral and tibial bone marrow from 12 wk-old female WT C57BL/6J mice and differentiated as described previously (28). After 7 d, BMDMs were seeded in RPMI1640 medium (Gibco) enriched with 10% Fetal Calf Serum (FCS; Biowest), 0.5% penicillin/streptomycin (P/S; Lonza), and 5% L929-conditioned medium (LCM; in house production as described by Weischenfeldt *et al.* (29)) at a density of 0.5 x 10^6 cells/mL in T175 culture flasks (13.5 x 10^6 cells in total). Subsequently, cells were either left unstimulated (naive; M0) or stimulated with LPS (100 ng/mL, Sigma-Aldrich) or IL-4 (20 ng/mL, PeproTech) for 6 h to skew BMDMs towards a disease- or repair-associated phenotype, respectively. Next, BMDMs were cultured in EV depleted culture medium (RPMI1640 supplemented with 10% FCS, 0.5% P/S, and 5% LCM, centrifuged overnight at 100,000 g at 4°C, followed by 0.2 µm filtration) and collected after 1 h (repeated four times). Next, EVs were pelleted using a differential centrifugation method. Briefly, collected supernatant was first centrifuged at 300 g for 10 min, then 10 min at 2,000 g, and finally 30 min at 10,000 g (all at 4°C). The supernatant was collected and centrifuged for 3 h at 115,000 g at 4°C using the XPN-80 ultracentrifuge equipped with a Ti70 rotor (Beckman). EV pellets were resolved in 1 mL ice-cold PBS (Gibco) and further purified by means of size exclusion chromatography (SEC). SEC was performed using chromatography columns (Bio-Rad Laboratories) filled with 10 ml Sepharose CL-2B beads (GE Healthcare). Sequential fraction 3.5 until 5.5 mL was collected from the flow-through and further upconcentrated using the Amicon Ultra 0.5 mL 10 kDa filter (Merck Millipore).

EV characterization – Western blotting and Nanoparticle Tracking Analysis (NTA) were used to characterize the BMDM-derived EVs. Detailed characterization procedure can be found in supplementary experimental procedures (SEP).

OPC isolation & culture – Cortices were isolated from WT C57BL/6J mouse pups (postnatal day 0-2; P0-P2) and enzymatically dissociated by a 20 min incubation with papain (3 U/mL, Sigma-Aldrich) diluted in Dulbecco's Modified Eagle Medium (DMEM; Gibco) supplemented with 1 mM L-cysteine (Sigma-Aldrich) at 37°C. Next, isolated mixed glial cells were cultured in DMEM enriched with 10% FCS and 1% P/S in poly-L-lysine (PLL, 5 µg/mL for 1 h at 37°C; Sigma-Aldrich) coated T75 culture flasks. Culture medium was changed on day 3, 7, and 10. From day 7, culture medium was supplemented with bovine insulin (5 µg/mL, Sigma-Aldrich) to promote OPC formation within mixed glial cell cultures. After 14 d, OPCs were isolated and seeded at a density of 300,000 cells/mL in differentiation medium as described by Tiane *et al.* (30), and treated daily with vehicle (PBS) or 4 x 10^8 EVs/mL for 6 d.

LC-ESI-MS/MS – Lipid extraction of LPS- and IL-4-stimulated BMDM-derived EVs was performed based on a Bligh and Dyer protocol, as described in Bogie *et al.* (31). Detailed instructions can be found in SEP.

Cholesterol measurements EVs – Cholesterol levels of EVs were determined using the Amplex Red Cholesterol Assay kit (Invitrogen) according to the manufacturer's instructions. Fluorescence was measured using the CLARIOstar PLUS microplate reader (BMG Labtech).

Cholesterol depletion/repletion IL-4/LPS EVs – IL-4-stimulated BMDM-derived EVs were depleted of cholesterol by incubation with 2.5% and 5% m/v methyl-ß-cyclodextrin (MßCD; Sigma-Aldrich) for 1 h at 37°C. LPS-stimulated BMDM-derived EVs were repleted of cholesterol by incubating the EVs with 2.5% and 5% m/v MßCD:cholesterol complexes (molar mass 8:1) overnight at 37°C while shaking at 250 rpm. After cholesterol depletion/repletion, EVs were purified to remove unincorporated MßCD and/or cholesterol and upconcentrated by means of SEC and Amicon filters, respectively.

EV internalization by OPCs – EVs were fluorescently labeled with 1,1'-dioctadecyl-3,3,3',3'-tetramethylindo-carbocyanine perchlorate (DiI; Sigma-Aldrich) for 30 min at 37°C and further purified to remove unincorporated DiI and upconcentrated, as described above. OPCs, either cultured on coverslips or not, were exposed to 4 x 10^8/mL DiI-labeled EVs for 3 h and subsequently washed with PBS to remove unincorporated DiI-labelled EVs. OPCs covered on coverslips were fixated with 4% paraformaldehyde (PFA; Sigma-Aldrich) for 30 min at room temperature (RT), counterstained with DAPI (Sigma-Aldrich) for 10 min, and imaged using the Leica DM2000 LED fluorescence microscope (Leica Microsystems). Similarly, OPCs not cultured on coverslips were collected and analyzed for fluorescence intensity using the FACSCalibur (BD Biosciences).

Cerebellar brain slice cultures – Cerebellar brain slices (BSCs) were obtained from P9-P10 WT C57BL/6 mouse pups and cultured as described previously (32, 33). After 3 d, BSCs were demyelinated with lysolecithin (0.5 mg/mL, Sigma-Aldrich) for 16 h. Next, BSCs were allowed to recover in culture medium for 1 d and treated daily with vehicle or 2 x 10^9 EVs/mL for 6 d, followed by immunohistochemical analysis.

Cuprizone-induced acute demyelination in vivo model – 8 wk-old male WT C57BL/6 mice were fed ad libitum a diet of 0.3% (w/w) cuprizone (bis[cyclohexanone]ox-aldihydrozone; Sigma-Aldrich) mixed in powdered standard chow for 5 wk to induce acute demyelination. Subsequently, mice were stereotaxically injected with M0, LPS-, or IL-4-stimulated BMDM-derived EVs. Briefly, the skull surface and the bregma served as the stereotaxic zero points. The cranium was perforated at ML -0.7 mm, AP 1.1 mm, and DV -2.0 mm. Using a Hamilton precision syringe (26G needle), 2 µL of M0, LPS, or IL-4 EVs, 1 x 10^9 EVs in total, was injected into the lateral ventricle as described in Facchinetti *et al.* (34). Next, mice were fed a normal chow for 1 wk and subsequently sacrificed. Tissue was collected for immunohistochemical analysis.

Immunofluorescence staining and image analysis – OPCs were cultured on glass cover slides and fixed in 4% PFA for 30 min at RT. BSCs were fixed in 4% PFA for 15 min at RT. Brain tissue of the cuprizone mice was isolated, snap-frozen, and sectioned with a Leica CM1900UV cryostat (Leica Microsystems) to obtain 10 µm slices. To stain OPCs, cells were first blocked for 30 min in blocking buffer (1% BSA in 0.05% PBS-Tween-

20; Millipore) at RT. Next, OPCs were incubated with relevant primary antibodies (Suppl. Table 1) diluted in blocking buffer for 4 h at RT. After washing, OPCs were incubated with relevant secondary antibodies (Suppl. Table 1) diluted in PBS for 1 h at RT. Finally, nuclei were counterstained with DAPI for 10 min, and coverslips were mounted with fluorescent mounting medium (Invitrogen). Immunostainings of BSCs and brain tissue were performed as described previously (28, 31). OPCs and cryosections were imaged using the Leica DM2000 LED fluorescence microscope, while an LSM 880 confocal microscope (Zeiss) was used to analyze BSCs. ImageJ was used to perform quantification of immunofluorescent images and to assess oligodendrocyte morphological complexity using the Sholl analysis. Representative images shown are digitally enhanced.

Luciferase-based nuclear receptor reporter assay – To determine the activation of LXRα or LXRß, a luciferase-based reporter assay was performed using the ONE-Glo Luciferase Assay System kit (Promega), as described previously (35). Briefly, COS7 cell lines were seeded in 60 mm dishes at a density of 550,000 cells/dish and transfected with 1.8 µg of plasmid DNA, including 0.2 µg pGAL4hLXRα or pGAL4hLXRβ, 1 µg pG5-TK-GL3, and 0.6 µg of pCMV-β-galactosidase, using JetPEI (Polyplus-transfection SA) as transfection reagent. After overnight incubation, 10,000 cells/well were seeded in a 96-well plate in DMEM medium enriched with 1% P/S. Next, cells were stimulated with vehicle (PBS) or 4 x 10^8, 8 x 10^8, or 4 x 10^9 EVs/mL for 24 h. Afterward, cells were lysed using lysis buffer, and luminescence was measured using the CLARIOstar PLUS microplate reader.

Statistical analysis – Data were statistically analyzed using GraphPad Prism v9 (GraphPad Software Inc.) and are reported as mean ± S.E.M. The D'Agostino and Pearson omnibus normality test was used to test for normal distribution. When the datasets were normally distributed, an ANOVA (Tukey's post hoc analysis) or two-tailed unpaired Student's *t*-test (with Welch's correction if necessary) was used to determine statistical significance between groups. When datasets are not normally distributed, the Kruskal-Wallis or Mann-Whitney analysis was performed. P-values < 0.05 were considered to indicate a significant difference between two groups (*, $P < 0.05$; **, $P < 0.01$; ***, $P < 0.001$; ****, $P < 0.0001$).

RESULTS

EVs released by RAMs promote OPC differentiation and maturation in vitro – Macrophages are abundantly found in MS lesions and can acquire both detrimental and beneficial phenotypes that suppress or promote OPC maturation and therefore remyelination, respectively (23, 31). Given that extracellular vesicles (EVs) are a significant component of specific cell-derived secretome and are shown to be associated with intercellular communication in disease pathology (36-38), we reasoned that repair-associated macrophages (RAM)-derived EVs could promote OPC maturation. First, EVs were isolated from naive (M0 EV), LPS-stimulated (LPS EV), and IL-4-stimulated (IL-4 EV) bone marrow-derived macrophages (BMDMs) and characterized according to the 2018 MISEV guidelines (39). Nanoparticle Tracking Analysis (NTA) was performed to identify the concentration and size of the BMDM-derived particles (Fig. 1**A**-**B**). The size of the EVs was 153.2 ± 2.3, 141.6 ± 5.7, and 157.8 ± 3.9 nm for M0 EVs, LPS EVs, and IL-4 EVs, respectively. These results reveal that the size and concentration distribution were similar for the isolated particles of all BMDM phenotypes and fit into the size range of small EVs (< 200 nm). Immunoblotting demonstrated the presence of the EV markers Flotillin 1, Annexin A2, and CD81 in M0 EVs, LPS EVs, and IL-4 EVs. Further, the endoplasmic marker GRP94, which is a marker underrepresented in EVs, was rather not expressed in all EVs (Fig. 1**C**). To summarize, these results confirm the successful isolation of EVs derived from BMDM cell culture media.

To establish the effect of BMDM-derived EVs on the maturation process of OPCs, *in vitro* OPC cultures were exposed to M0 EVs, LPS EVs, and IL-4 EVs. By using flow cytometry, we observed that the three EV types were efficiently internalized by OPCs (Fig. S1**A**). The uptake of EVs was confirmed using fluorescence microscopy (Fig. S1**B**). Next, immunostaining demonstrated that IL-4 EVs enhance OPC maturation compared to vehicle-, M0 EV-, and LPS EV-treated OPCs, as evidenced by an increased ratio of the mature oligodendrocyte marker MBP over the pre-oligodendrocyte marker O4 (Fig. 1**D**-**E**).

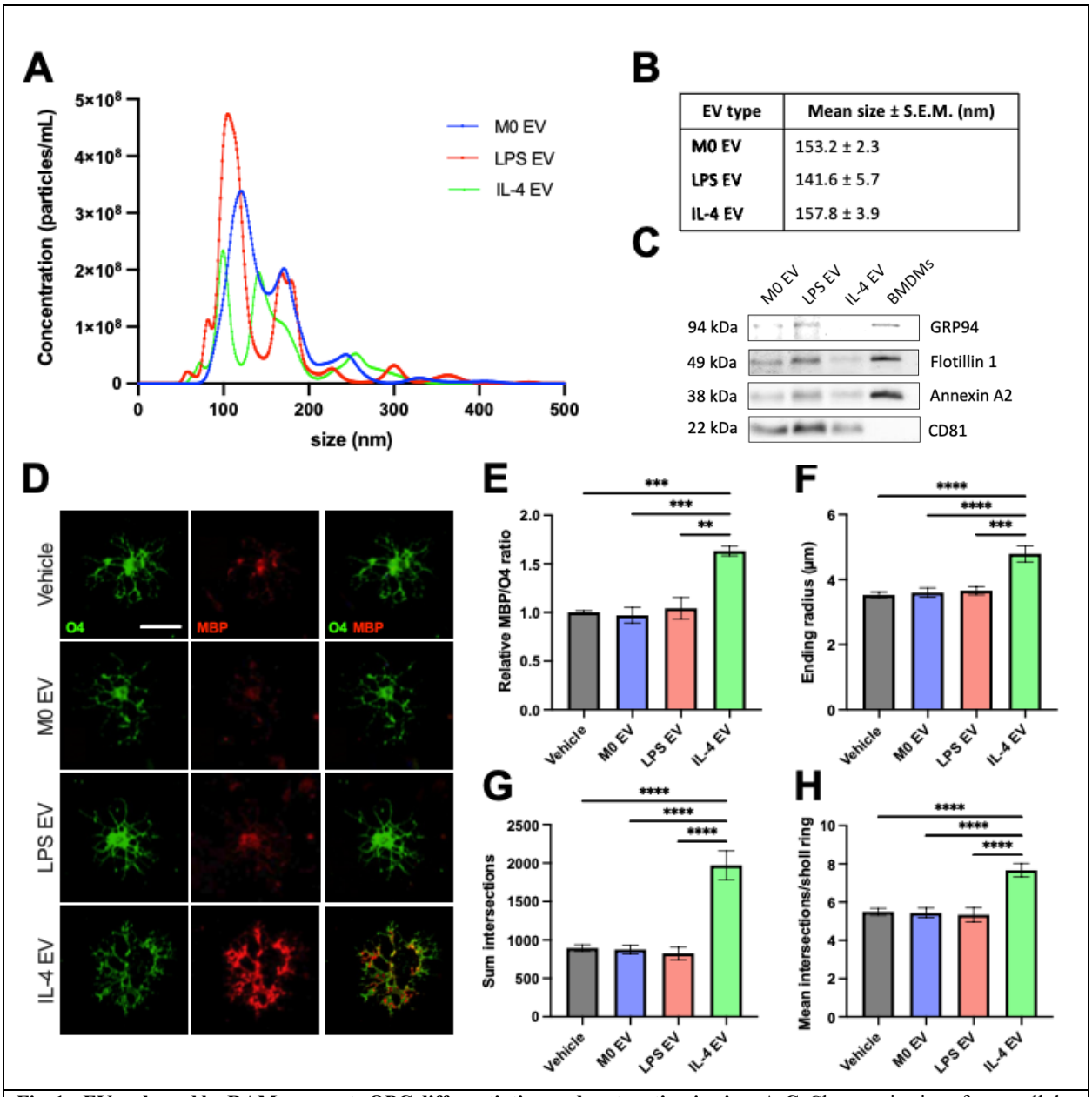

Fig. 1 – **EVs released by RAMs promote OPC differentiation and maturation *in vitro***. **A-C**: Characterization of extracellular vesicles (EVs) produced by bone marrow-derived macrophages (BMDMs) with different phenotypes. Particle size profile distribution (A) and mean size (B) of particles isolated from naive (M0 EV), LPS-stimulated (LPS EV), and IL-4-stimulated (IL-4 EV) BMDM culture medium as measured by Nanoparticle Tracking Analysis (NTA). Western blot analysis (C) of EV markers Flotillin 1, Annexin A2, CD81, and underrepresented EV marker GRP94 of M0 EVs, LPS EVs, and IL-4 EVs. **D-E**: Representative immunocytochemical images (D) and relative quantification of the MBP/O4 ratio (E) of oligodendrocyte progenitor cells (OPCs) stimulated with vehicle (PBS), M0 EVs, LPS EVs, and IL-4 EVs (4 x 10^8 EVs/mL) for 6 d (n = 5 wells; scale bar, 15 µm). **F-H**: Morphological analysis by means of Sholl analysis of OPCs treated with vehicle, M0 EVs, LPS EVs, or IL-4 EVs (4 x 10^8 EVs/mL) for 6 d with ending radius (F), sum of intersections (G), and mean intersections per Sholl ring (H) as read-out parameter (n = 5 wells; 15-30 cells per condition). All data are represented as mean ± S.E.M. **, P < 0.01; ***, P < 0.001; ****, P < 0.0001; one-way ANOVA.

To confirm increased maturation of OPCs upon IL-4 EV exposure, cell morphology was studied by means of the Sholl analysis. Here, we observed that IL-4 EV-stimulated OPCs acquired a more complex morphology as indicated by an increased ending radius, sum of intersections, and mean intersections

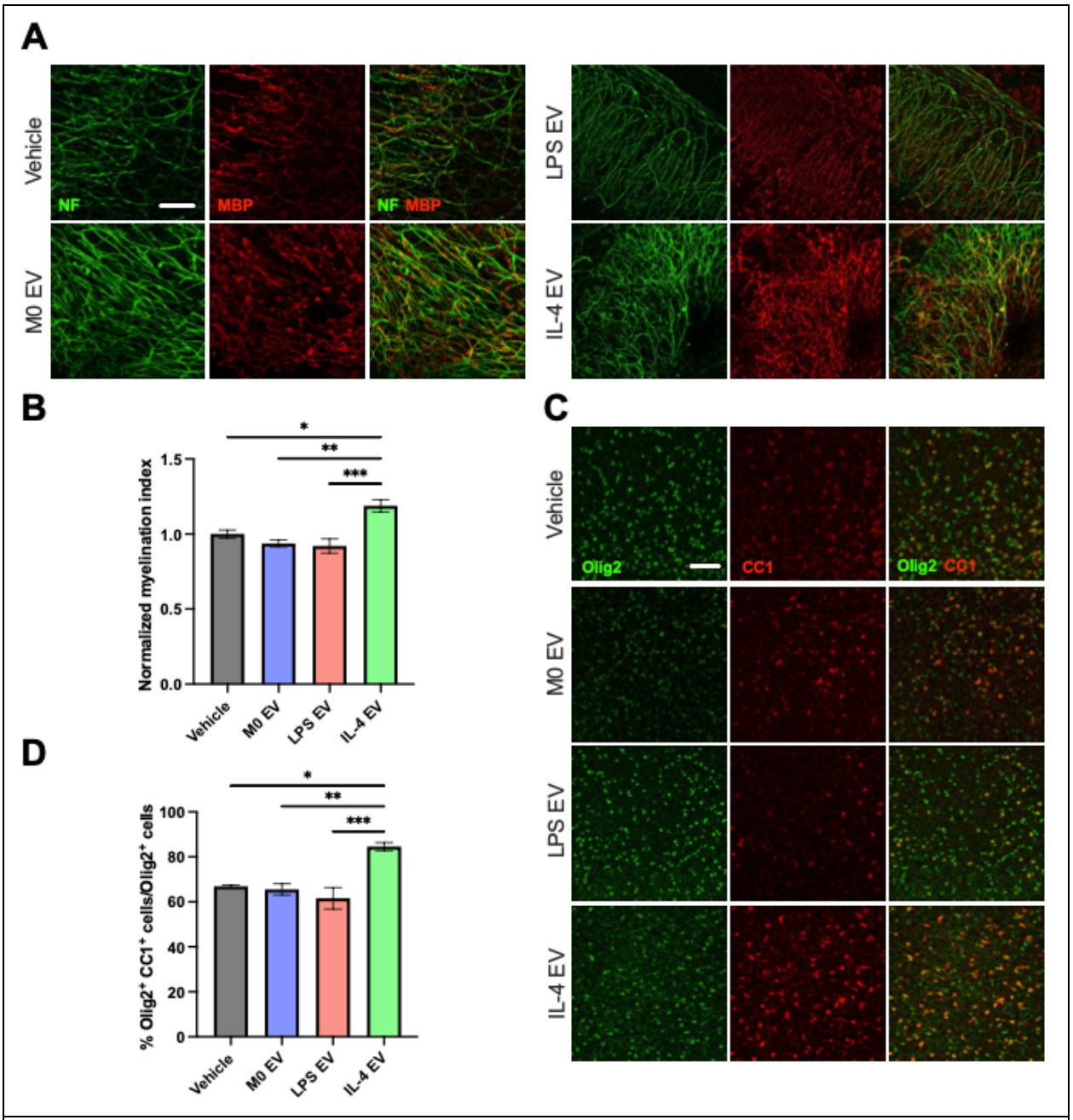

Fig. 2 – **EVs released by RAMs promote remyelination in an *ex vivo* cerebellar brain slice model**. **A-B**: Representative images (A) of immunofluorescence MBP and neurofilament (NF) staining of *ex vivo* cerebellar brain slice cultures treated with vehicle (PBS) or extracellular vesicles (EVs) derived from naive (M0 EV), LPS-stimulated (LPS EV), or IL-4-stimulated (IL-4 EV) bone marrow-derived macrophages (2 x 10^9 EVs/mL) for 6 d (scale bar, 50 µm). Normalized quantification of MBP^+ NF^+ axons out of total NF^+ axons in *ex vivo* cerebellar brain slices (B) treated with vehicle, M0 EVs, LPS EVs, or IL-4 EVs (2 x 10^9 EVs/mL) for 6 d (n = 6 slices). **C-D**: Representative images (C) of immunofluorescence Olig2 and CC1 staining of *ex vivo* cerebellar brain slice cultures treated with vehicle, M0 EVs, LPS EVs, or IL-4 EVs (2 x 10^9 EVs/mL) for 6 d. Quantification of percentage $Olig2^+$ $CC1^+$ cells out of $Olig2^+$ cells in *ex vivo* cerebellar brain slices (D) treated with vehicle, M0 EVs, LPS EVs, or IL-4 EVs (2 x 10^9 EVs/mL) for 6 d (n = 6 slices; scale bar, 50 µm). All data are represented as mean ± SEM. *, $P < 0.05$; **, $P < 0.01$; ***, $P < 0.001$; one-way ANOVA.

per Sholl ring, which is associated with more mature oligodendrocytes (Fig. 1**F-H**). Of interest, LPS EVs did not prevent OPC differentiation compared to vehicle-treated and M0 EV-treated OPCs (Fig. 1**D-H**). Overall, these results demonstrate that RAM-like IL-4-stimulated

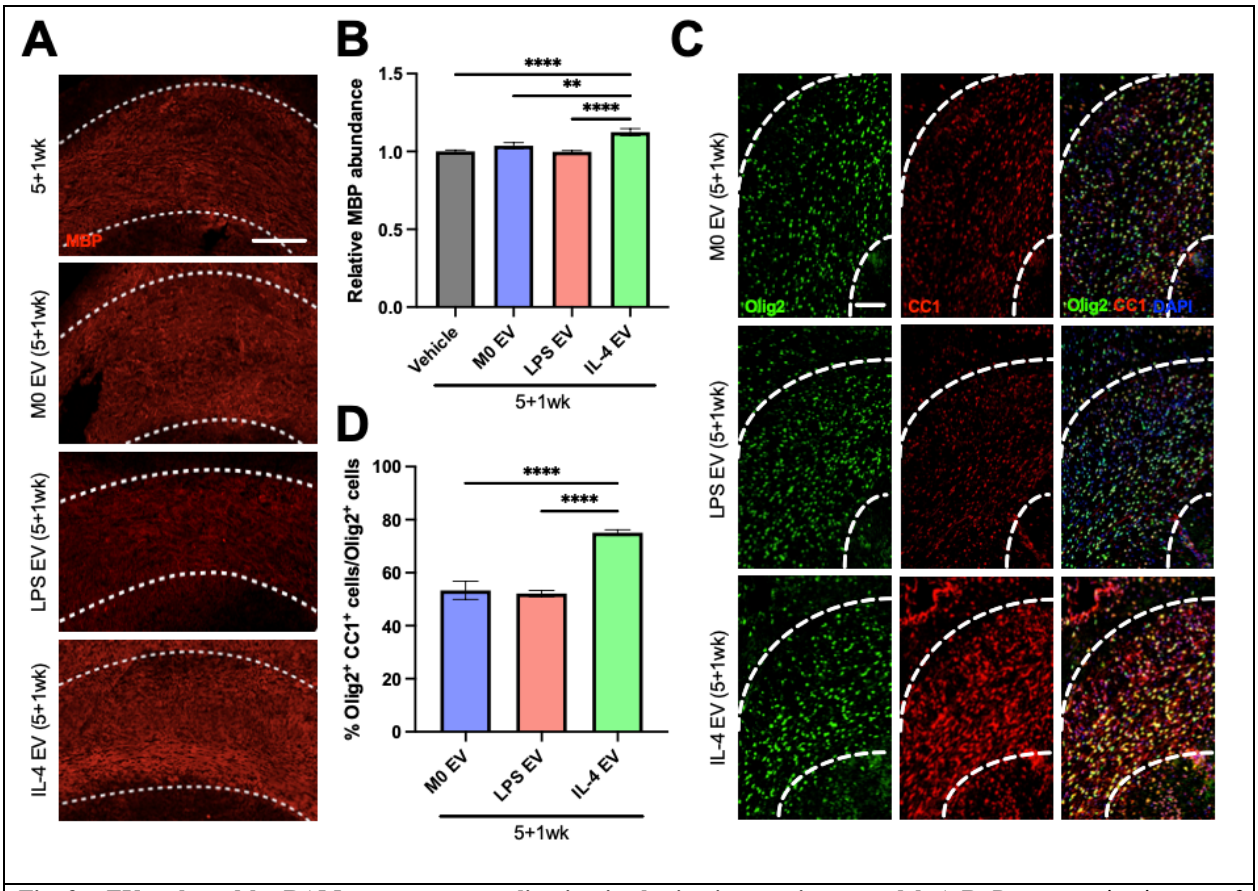

Fig. 3 – **EVs released by RAMs promote remyelination in the *in vivo* cuprizone model**. **A-B**: Representative images of immunofluorescence MBP staining (A) of the corpus callosum (CC) from mice stereotaxically injected with vehicle (PBS) or extracellular vesicles (EVs) derived from naive (M0 EV), LPS-stimulated (LPS EV), or IL-4-stimulated (IL-4 EV) bone marrow-derived macrophages (1 x 10^9 EVs) after five weeks of cuprizone-induced demyelination (5wk) and analyzed after one week of subsequent remyelination (5+1wk). The outer border of the CC is lined with a dotted line (scale bar, 150 µm). Quantification of the MBP^+ area (B) of the CC from vehicle-, M0 EV-, LPS EV-, or IL-4 EV-treated mice after 5+1wk (n = 5-6 mice/group) **C-D:** Representative images of immunofluorescence Olig2 and CC1 staining of the CC from mice stereotaxically injected with vehicle, M0 EVs, LPS EVs, or IL-4 EVs (C) after five weeks in an *in vivo* cuprizone model and analyzed after one week of subsequent remyelination (5+1wk). The outer border of the CC is lined with a dotted line (scale bar, 75 µm). Quantification of the percentage $Olig2^+$ $CC1^+$ cells out of $Olig2^+$ cells (D) of the CC from M0 EV-, LPS EV-, or IL-4 EV-treated mice after 5+1wk (n = 5-6 mice/group). All data are represented as mean ± SEM. **, P < 0.01; ****, P < 0.0001; one-way ANOVA.

BMDMs promote the differentiation of OPCs *in vitro* by secreting EVs.

EVs released by RAMs promote remyelination ex vivo and in vivo – To investigate the effect of BMDM-derived EVs on remyelination, *ex vivo* cerebellar brain slice cultures (BSCs) were demyelinated with lysolecithin and subsequently treated with vehicle, M0 EVs, LPS EVs, or IL-4 EVs (Fig. S2**A**). Immunostaining demonstrated that IL-4 EVs promote remyelination *ex vivo*, as indicated by an increased colocalization of myelin (MBP) and axons (neurofilament; NF) (Fig. 2**A-B**). Accordingly, a higher percentage of $CC1^+$ cells (mature oligodendrocytes) within the $Olig2^+$ oligodendroglial lineage cells was found in BSCs treated with IL-4 EVs (Fig. 2**C-D**). Interestingly, similar to *in vitro* OPC cultures, BSCs stimulated with LPS EVs did not show impaired remyelination compared to vehicle- or M0 EV-treated BSCs. (Fig. 2**A-D**).

To evaluate the significance of these *ex vivo* results, the cuprizone-induced de- and remyelination model was used. Cuprizone is a copper-chelating agent that induces oligodendroglial cell death, resulting in demyelination in distinct brain regions such as the corpus callosum (CC). After termination of cuprizone administration, spontaneous remyelination occurs, as demonstrated by an MBP immunostaining of the CC of animals after demyelination (5wk) and after remyelination (5+1wk) (Fig. S2**B-D**). Animals that were

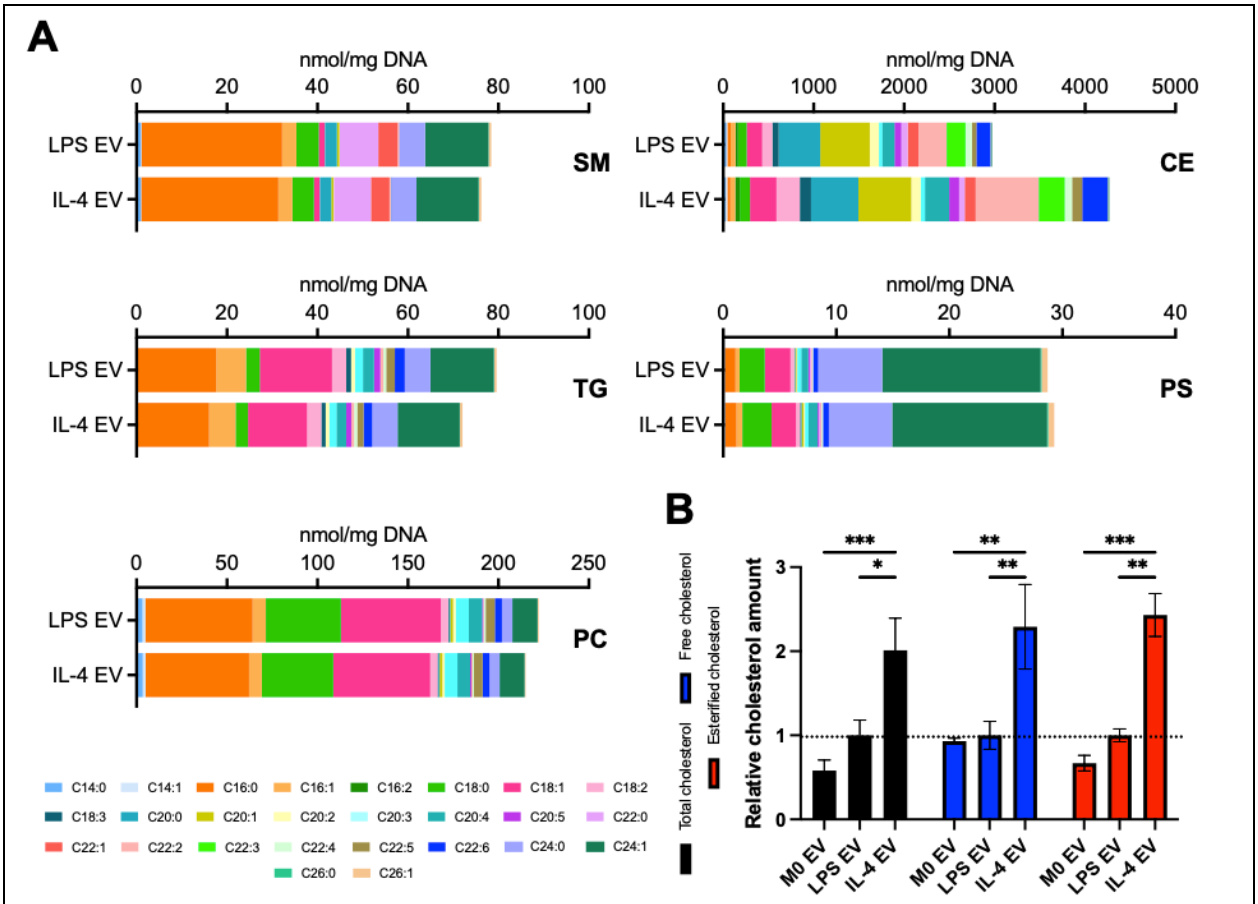

Fig. 4 – **EVs derived from RAMs contain elevated cholesterol levels**. **A**: Liquid chromatography-electrospray tandem mass spectrometry (LC-ESI-MS/MS) analysis of extracellular vesicles (EVs) derived from LPS-stimulated (LPS EV) or IL-4-stimulated (IL-4 EV) bone marrow-derived macrophages of the most common lipid species present in BMDM-derived EVs of sphingomyelin (SM), cholesterol ester (CE), triglycerides (TG), phosphatidylserine (PS), and phosphatidylcholine (PC) (n = 3 isolations). **B**: Quantification of relative total cholesterol, free cholesterol, and cholesterol ester levels by means of the Amplex red cholesterol assay of M0 EVs, LPS EVs (dotted line), and IL-4 EVs (n = 4 biological replicates). All data are represented as mean ± SEM. *, $P < 0.05$; **, $P < 0.01$; ***, $P < 0.001$; one-way ANOVA.

stereotaxically injected into the lateral ventricle with IL-4 EVs show markedly increased MBP abundance in the CC during remyelination compared to animals that were injected with vehicle, M0 EVs, or LPS EVs (Fig. 3**A-B**). Consistent with these findings, immunostaining for Olig2 and CC1 demonstrated enhanced OPC differentiation and maturation in the CC of mice exposed to EVs released by IL-4-stimulated BMDMs, as reflected by a significant increase in the percentage of $Olig2^+$ $CC1^+$ cells/$Olig2^+$ cells (Fig. 3**C-D**). LPS EVs did not affect OPC maturation and remyelination in the *in vivo* cuprizone model compared to vehicle- or M0 EV-treated mice. Altogether, these findings indicate that EVs released by BMDMs with a RAM-like phenotype enhance remyelination in the *ex vivo* cerebellar BSC and *in vivo* cuprizone model by stimulating OPC differentiation and maturation.

Increased cholesterol levels underlie the reparative impact of EVs released by RAMs in vitro – So far, we have demonstrated that IL-4 EVs promote OPC differentiation and maturation *in vitro*, and enhance remyelination *ex vivo* and *in vivo*. However, it remains unknown which factors are responsible for these repair processes. Emerging evidence indicates that lipids control OPC maturation and remyelination (40-43). Therefore, we defined the lipid profile of the EVs produced by DAMs and RAMs. Liquid chromatography-electrospray ionization tandem mass spectrometry (LC-ESI-MS/MS) demonstrated no significant differences in sphingomyelin (SM), triglycerides (TG), phosphatidylserine (PS), and phosphatidylcholine (PC) levels in EVs released by LPS- and IL-4-stimulated BMDMs. Interestingly, when comparing the cholesterol ester (CE) levels in both EV types, a marked increase was observed in

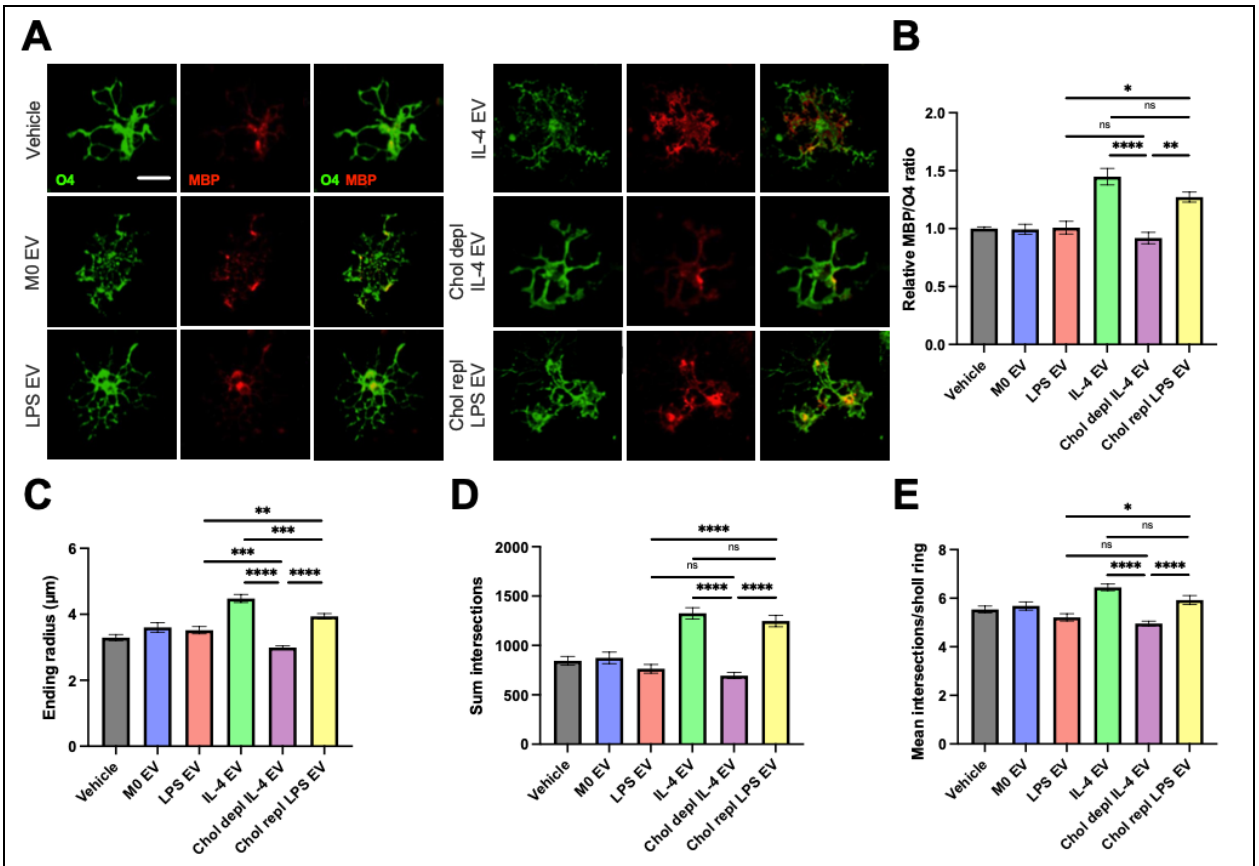

Fig. 5 – Increased cholesterol levels underlie the reparative impact of EVs released by RAMs *in vitro*. **A-B**: Representative immunocytochemical images (A) and relative quantification of the MBP/O4 ratio (B) of oligodendrocyte progenitor cells (OPCs) stimulated with vehicle (PBS), or EVs produced by naive (M0 EV), LPS-stimulated (LPS EV), IL-4-stimulated (IL-4 EV) bone marrow-derived macrophage-derived, and cholesterol depleted IL-4 EVs (Chol depl IL-4 EV) or cholesterol repleted LPS EVs (Chol repl LPS EV) (4 x 10^8 EVs/mL) for 6 d (n = 7 wells; scale bar, 10 µm). **C-E**: Morphological analysis by means of Sholl analysis of OPCs treated with vehicle, M0 EVs, LPS EVs, IL-4 EVs, cholesterol depleted IL-4 EVs, or cholesterol repleted LPS EVs (4 x 10^8 EVs/mL) for 6 d with ending radius (C), sum of intersections (D), and mean intersections per Sholl ring (E) as read-out parameter (n = 7 wells; 15-30 cells per condition). All data are represented as mean ± SEM. Non-significant (ns), $P > 0.05$; *, $P < 0.05$; **, $P < 0.01$; ***, $P < 0.001$; ****, $P < 0.0001$; one-way ANOVA.

IL-4 EVs (Fig. 4**A**). Increased levels of CE in IL-4 EVs were confirmed using the Amplex Red cholesterol assay. Additionally, our results reveal that the CE levels and the amount of total cholesterol are elevated in IL-4 EVs compared to M0 EVs and LPS EVs (Fig. 4**B**).

Several studies indicate that cholesterol is essential for efficient OPC maturation and proper remyelination (40, 44-47). To verify the essential role of cholesterol associated with EVs released by RAMs in OPC differentiation, we next aimed to define whether depletion of EV-associated cholesterol impairs the reparative features of EVs released by RAMs. To this end, IL-4 EVs were first incubated with different concentrations (0%, 2.5%, 5% m/v) of the cholesterol removing agent methyl-ß-cyclodextrin (MßCD). 2.5% m/v MßCD appeared to be the most efficient to achieve cholesterol-depleted IL-4 EVs without affecting cellular uptake (Fig. S3**A-C**). Next, *in vitro* OPC cultures were treated with vehicle, M0 EVs, LPS EVs, IL-4 EVs, and cholesterol-depleted IL-4 EVs (Chol depl IL-4 EV). Immunofluorescence analysis demonstrated that cholesterol depletion nullifies the pro-regenerative impact of EVs released by RAMs in OPC cultures (Fig. 5**A-B**). Mirroring these findings, Sholl analysis demonstrated that OPCs treated with cholesterol-depleted IL-4 EVs show a reduced morphological complexity as demonstrated by a decreased ending radius, sum of intersections, and mean intersections per Sholl ring (Fig. 5**C-E**). As a proof-of-concept, we next aimed to verify whether cholesterol replenishment of LPS EVs (Chol repl LPS EV) induces OPC maturation.

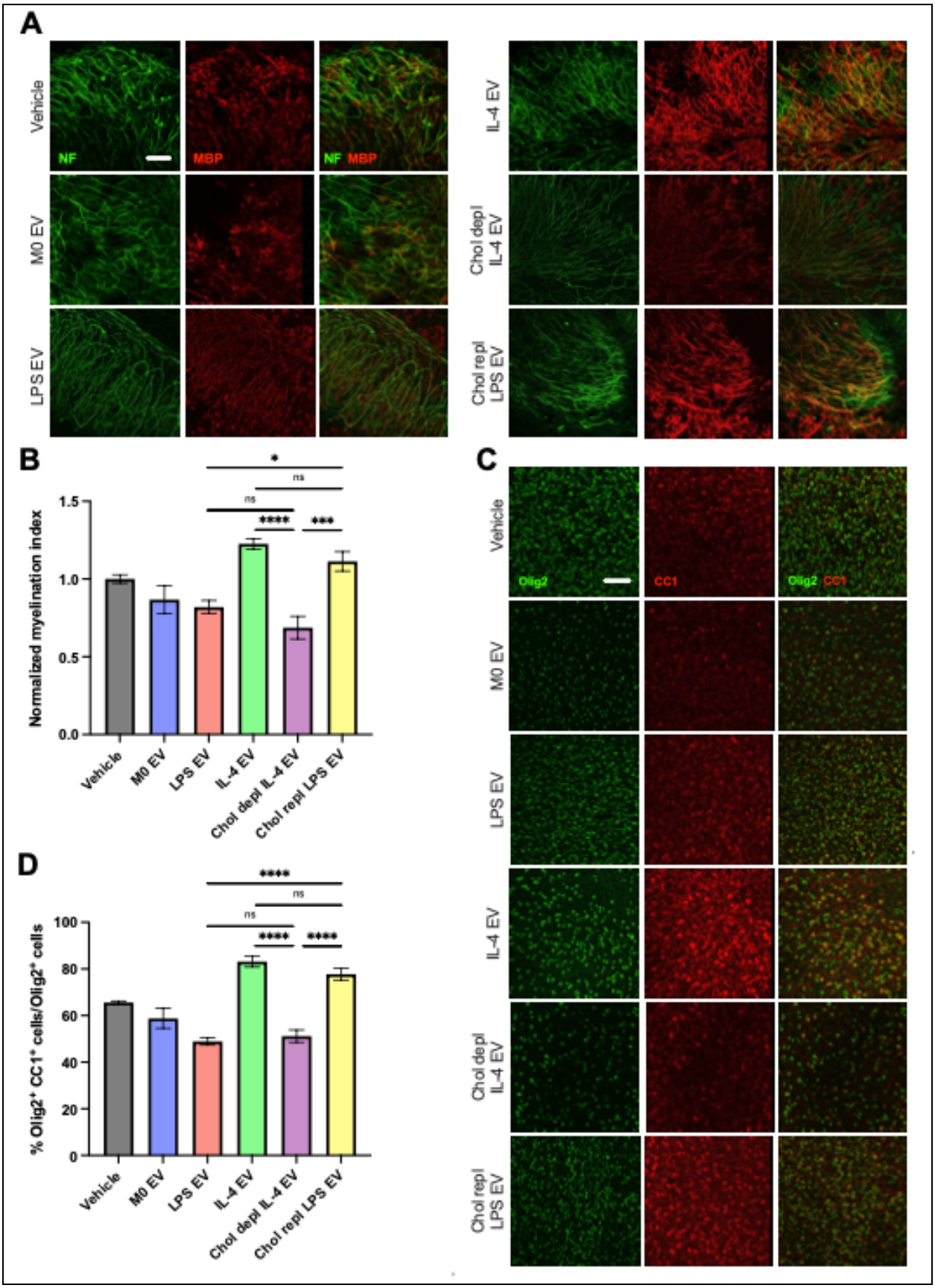
A
Vehicle
M0 EV
LPS EV
IL-4 EV
Chol depl IL-4 EV
Chol repl LPS EV
NF
MBP
NF MBP
B
Normalized myelination index
1.5
1.0
0.5
0.0
*
ns
ns
****
***
Vehicle
M0 EV
LPS EV
IL-4 EV
Chol depl IL-4 EV
Chol repl LPS EV
C
Olig2
CC1
Olig2 CC1
D
% Olig2+ CC1+ cells/Olig2+ cells
100
80
60
40
20
0
****
ns
ns
****
****

Fig. 6 – **Increased cholesterol levels underlie the reparative impact of EVs released by RAMs in *ex vivo* cerebellar brain slice model**. **A-B**: Representative images (A) of immunofluorescence MBP and neurofilament staining of *ex vivo* cerebellar brain slice cultures treated with vehicle or extracellular vesicles (EVs) derived from naive (M0 EV), LPS-stimulated (LPS EV), or IL-4-stimulated (IL-4 EV) bone marrow-derived macrophages, and cholesterol depleted IL-4 EVs (Chol depl IL-4 EV) or cholesterol repleted LPS EVs (Chol repl LPS EV) (2 x 10^9 EVs/mL) for 6 d (scale bar, 50 µm). Normalized quantification of MBP^+ NF^+ axons out of total NF^+ axons in *ex vivo* cerebellar brain slices (B) treated with vehicle, M0 EVs, LPS EVs, IL-4 EVs, cholesterol depleted IL-4 EVs, or cholesterol depleted LPS EVs (2 x 10^9 EVs/mL) for 6 d (n = 6 slices). **C-D**: Representative images (C) of immunofluorescence Olig2 and CC1 staining of *ex vivo* cerebellar brain slice cultures treated with vehicle, M0 EVs, LPS EVs, IL-4 EVs, cholesterol depleted IL-4 EVs, or cholesterol repleted LPS EVs (2 x 10^9 EVs/mL) for 6 d. Quantification of percentage $Olig2^+$ $CC1^+$ cells out of $Olig2^+$ cells in *ex vivo* cerebellar brain slices (D) treated with vehicle, M0 EVs, LPS EVs, IL-4 EVs, cholesterol depleted IL-4 EVs, or cholesterol repleted LPS EVs (2 x 10^9 EVs/mL) for 6 d (n = 6 slices; scale bar, 50 µm). All data are represented as mean ± SEM. Non-significant (ns), $P > 0.05$; *, $P < 0.05$; ***, $P < 0.001$; ****, $P < 0.0001$ one-way ANOVA.

LPS EVs were exposed to 2.5% and 5% m/v MßCD:cholesterol complexes. In line with cholesterol depletion of IL-4 EVs, 2.5% m/v MßCD:cholesterol successfully replenished LPS EVs with cholesterol without affecting cellular uptake (Fig. S3**D-F**). In contrast to LPS EVs and cholesterol-depleted IL-4 EVs, OPCs stimulated with cholesterol-repleted LPS EVs showed increased differentiation and maturation to the same degree as IL-4 EV-treated OPCs, as reflected by a higher MBP/O4 ratio and increased morphological complexity as determined by the Sholl analysis (Fig. 5**A-E**). Taken these results together, EVs derived from RAM-like BMDMs promote OPC differentiation and maturation *in vitro* in a cholesterol-dependent manner.

Increased cholesterol levels underlie the reparative impact of EVs released by RAMs ex vivo – Next, we investigated the pro-regenerative impact of cholesterol transported by IL-4 EVs in *ex vivo* cerebellar BSCs. In line with OPC cultures, cholesterol depletion of IL-4 EVs markedly decreased endogenous remyelination in BSCs, as indicated by a decrease of myelinated axons (MBP^+ NF^+ axons/NF^+ axons) (Fig. 6**A-B**). In support of the latter finding, cholesterol-repleted LPS EVs enhanced remyelination compared to LPS EVs and cholesterol-depleted IL-4 EVs and even to the same degree as IL-4 EVs (Fig. 6**A-B**). To further demonstrate the ability of OPCs to differentiate into mature oligodendrocytes contributing to remyelination, BSCs were stained with Olig2 and CC1 antibodies. Immunohistochemical analysis revealed a significant reduction in the percentage of $Olig2^+$ $CC1^+$ cells/$Olig2^+$ cells for BSCs treated with cholesterol-depleted IL-4 EVs compared to BSCs treated with IL-4 EVs (Fig. 6**C-D**). In addition, LPS EVs or cholesterol-depleted IL-4 EVs did not promote differences in OPC differentiation and thus remyelination *ex vivo*, while cholesterol-repleted LPS EVs do stimulate OPC maturation and remyelination (Fig. 6**A-D**). Altogether, these results indicate that cholesterol present in EVs produced by RAM-like BMDMs is a crucial factor in promoting OPC differentiation and enhancing remyelination in an *ex vivo* cerebellar brain slice model.

EVs released by RAMs do not promote OPC maturation by activating LXRs – By using ligand-binding luciferase reporter assays, we next aimed to investigate whether IL-4 EVs and cholesterol repletion of LPS EVs promote ligation of LXRα and/or LXRß in OPCs, which are nuclear receptors that sense cellular cholesterol levels and are closely associated with OPC maturation and remyelination. Therefore, COS7 cells were exposed to 4 x 10^8, 8 x 10^8, and 4 x 10^9 EVs/mL. While the synthetic LXR agonist T0901317 (10 µM) showed an increased LXRα/ß activity, none BMDM-derived EVs activated LXRα or LXRß (Fig. 7**A-B**). Consequently, we suggest that IL-4 EVs promote OPC differentiation and maturation in an LXR-independent way.

DISCUSSION

Macrophages are abundantly present in active MS lesions and can have detrimental or beneficial functions during disease course (6, 8, 10). To date, however, the communication between macrophages and OPCs still remains to be clarified. Here, we demonstrate that EVs released by RAMs promote OPC differentiation and enhance remyelination. Importantly, cholesterol levels were found to be a key determinant of the reparative impact of RAM-associated EVs, with high cholesterol levels being associated with remyelination. Vice versa, cholesterol replenishment of DAM-derived EVs stimulates

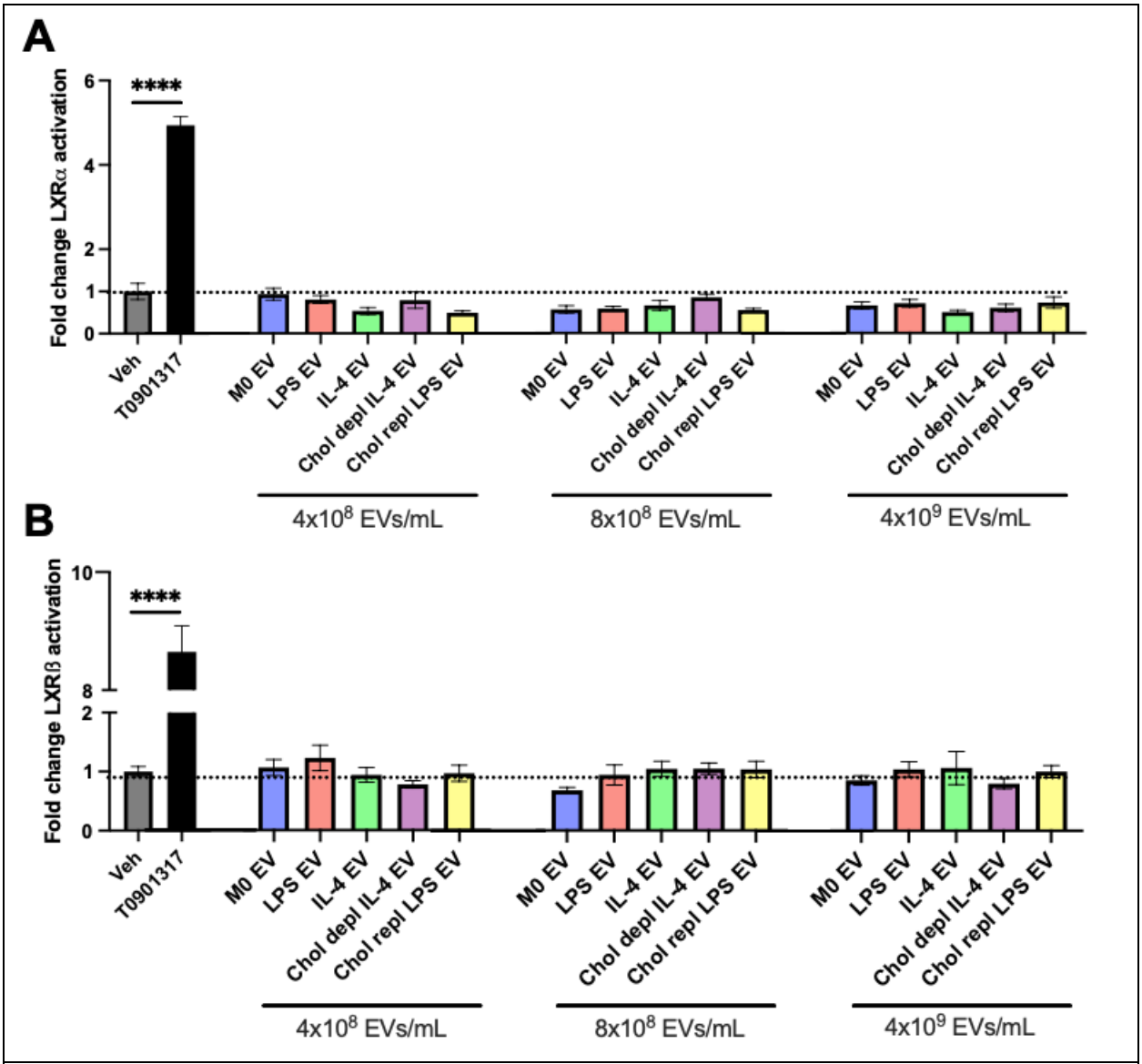

Fig. 7 – **EVs released by RAMs do not promote OPC maturation by activating**. **A-B**: Luciferase-based reported assay assessed to investigate LXRα (A) and LXRß (B) activity in COS7 cells stimulated for 24 h with vehicle (PBS) or extracellular vesicles (EVs) derived from naive (M0 EV), LPS-stimulated (LPS EV), IL-4-stimulated (IL-4 EV) bone marrow-derived macrophages, and cholesterol depleted IL-4 EVs (Chol depl IL-4 EV), cholesterol repleted LPS EVs (Chol repl LPS EV) (different concentrations of EVs, indicated in the figure), and the selective LXR agonist T0901317 (10 µM) (n = 6 wells). All data are represented as mean ± SEM. ****, $P < 0.0001$; Student's t-test (T0901317), one-way ANOVA.

OPC differentiation and accompanying remyelination. Thus, our findings show that cholesterol in macrophage-derived EVs drives remyelination in the brain by stimulating OPC differentiation towards mature, myelinating oligodendrocytes.

We demonstrate that RAMs induce a repair-permissive microenvironment by secreting EVs. Failure of OPC differentiation and remyelination is a typical characteristic of the progressive nature of demyelinating diseases, such as MS (48, 49). Remyelination relies on the proper proliferation and migration of OPCs towards MS lesions, where they differentiate into mature oligodendrocytes and subsequently synthesize new myelin sheaths (50). This process can be influenced by various factors present in the lesion microenvironment, such as neurotrophic factors and inhibitory molecules (16, 51, 52). In MS, macrophages are known to contribute to disease progression and resolution depending on their phenotype. In particular, Miron *et al.* show that OPC proliferation and migration

were increased by the secretome of both DAMs and RAMs. However, only the RAM-derived secretome promoted OPC differentiation, thereby assisting in CNS repair (23). More specifically, the reparative effects of RAMs are at least partly dependent on the release of neurotrophic factors such as TGF-ß, IGF1, and CNTF (23, 53). Miron *et al.* further demonstrated that the capacity of OPCs to differentiate towards myelinating oligodendrocytes is promoted by activin A, a glycoprotein secreted by RAMs (23). Another recent study shows that repair-associated microglia stimulate OPC maturation in part via the production of IGF-I and downregulation of TNF-α (54). Together, these studies emphasize that the secretome of lesion-associated macrophages and microglia controls their disease-promoting and -resolving properties.

Recently, EVs have gained significant interest since they appear to play an essential role in the pathophysiology and resolution of several diseases (26, 36, 37, 55). For instance, in prostate cancer, AKT1-containing cancer cell-derived EVs facilitate tumor progression by modulating complex signaling networks, such as the MYC pathway, thereby affecting neighboring healthy cells (56). In contrast, dendritic cell (DC)-derived EVs prevent tumor growth as they contain major histocompatibility complex class I (MHC-I) and class II (MHC-II) proteins that induce cytotoxic T cell activation upon exposure to tumor peptides (57). Additionally, EVs are shown to be detrimental to the pathology of the autoimmune disease systemic lupus erythematosus (SLE). The number of T cell-derived EVs was found to be increased in serum samples derived from SLE patients compared to healthy controls, thereby contributing to chronic immune activation via type I IFN-signaling and excessive cytokine/chemokine response (58). Finally, the role of EVs in the pathophysiology of CNS disorders is growing rapidly. More specifically, in prion disease, misfolded prion proteins are transported to neighboring cells via EVs, thereby stimulating a cascade of further production of affected prion proteins (59, 60). In demyelinating disorders, the importance of EVs is illustrated by an altered ability to induce remyelination upon differentially conditioned microglia-derived EV stimulation (24). Likewise, our results now provide a new understanding of macrophage-derived EV-associated communication contributing to CNS repair in demyelinating disorder.

By using *in vitro* and *ex vivo* models, we demonstrate that the pro-regenerative impact of RAM-derived EVs is at least partly attributed to increased cholesterol levels present in these EVs. It has previously been reported that lipids are key mediators of remyelination, which is not surprising as the dry weight of myelin consists of approximately 70-85% of lipids (61). Furthermore, according to Dimas *et al.*, fatty acid synthesis by fatty acid synthase (FASN) is essential for efficient OPC differentiation and proper remyelination (41). In addition, Berghoff *et al.* show that cholesterol synthesis in neuronal cells is indispensable to induce proper CNS repair (45). Other research reports that oligodendrocyte formation is driven by 8,9-unsaturated sterols (40). However, lipids can also be transported via EVs functioning as transport vehicle between donor and recipient cells (62). EV-associated lipids provide an emerging diagnostic and potential therapeutic value and insight into the pathology of several peripheral diseases such as cancer and asthma (63-65). For instance, Nishida-Aoki *et al.* defined that EVs derived from highly metastatic cancer cells contain more unsaturated diacylglycerols (DG) compared to EVs from lower-metastatic cells. In addition, they demonstrated that DG-enriched EVs can activate the protein kinase D signaling pathway in endothelial cells leading to increased angiogenesis (64). Given the importance of lipid metabolism in cellular processes in the brain (66, 67), it is not surprising that EV-associated lipids can exert a detrimental or beneficial role in CNS disorders, e.g., Alzheimer's disease, Parkinson's disease (PD), and MS (68-70). As demonstrated by Grey *et al.*, EV-associated lipids released by N2a neuroblastoma cells impact the formation of α-synuclein plaques during PD by boosting α-synuclein oligomerization (68). Of the most prevalent lipids classes present in EVs, we defined that EV-associated cholesterol is at least partly responsible for enhanced remyelination in demyelinating diseases (71, 72). Cholesterol is a major component of myelin - up to 40% of all myelin lipids is cholesterol - and is essential to induce proper remyelination (42, 61). Of interest, in a recent study, it is observed that a dietary cholesterol intake increases OPC maturation and subsequently enhances remyelination in a cuprizone-induced demyelination mouse model.

Notably, dietary cholesterol supplementation did not affect inflammation *in vivo*, as defined using the experimental autoimmune encephalomyelitis (EAE) mouse model (44). Given that EVs also carry other bioactive molecules than lipids, such as nucleic acids and proteins (25), we cannot exclude that the cargo of EVs produced by macrophages with a repair-promoting phenotype has synergetic effects to stimulate remyelination. Activin A, for instance, is secreted by RAMs (23) and might be present in RAM-derived EVs assisting in CNS repair. In addition, the anti-inflammatory cytokine IL-4 can also have beneficial effects during CNS repair when present in the EVs released by RAMs (73). However, by depleting and repleting cholesterol from DAM- and RAM-derived EVs, respectively, we show that cholesterol is the rate-limiting factor in promoting remyelination upon disease- and repair stages in demyelinating diseases.

Cholesterol depletion is a well-established method to investigate the impact of cholesterol on different molecular mechanisms in health and disease. MßCD is the most commonly used tool to extract cholesterol from cells (74, 75). When incubating the DAM-derived EVs with a higher % m/v MßCD, the cellular uptake of EVs by OPCs decreases dramatically. Given that MßCD forms an MßCD-dimer, integrates into the cell membrane, and extracts the cholesterol from the membrane (74), the decreased cellular uptake might be due to reduced EV membrane stability. MßCD cannot only be used to deplete cholesterol from the cell membrane; however, in a mixture with cholesterol, it is also capable of enriching cell membranes with cholesterol (76). Depleting and even to further extend repleting cholesterol in EVs is rather novel and has not been performed in the past. Eventually, we successfully depleted cholesterol from RAM-derived EVs and replenished cholesterol in DAM-derived EVs using MßCD as a membrane-modulating tool.

Cholesterol homeostasis is regulated by a feed-forward system that LXRs provide by activating genes involved in cholesterol efflux (77, 78). Specific oxysterols and sterols, e.g., 24S-hydroxycholesterol, 25-hydroxycholesterol, 27-hydroxycholesterol, positively regulate the transcriptional activities of LXRs (79, 80). Several studies indicate that activation of LXRα and LXRß is correlated with enhanced OPC differentiation and remyelination (81-83). Surprisingly, in our study, we observe that macrophage-derived EVs with high cholesterol levels (e.g., IL-4 EVs, cholesterol-repleted LPS EVs) do not activate LXRs *in vitro*. Therefore, our results suggest there are other possible routes how EV-associated cholesterol derived from RAM-like macrophages improve OPC differentiation and remyelination. Given the fact that uptake of EVs by recipient cells is mediated by different mechanisms (84), it might be that RAM-derived EVs directly fuse with the cell membrane of OPCs, directly providing cells with cholesterol needed for efficient differentiation and myelin sheath formation. Another study reports that cholesterol facilitates signal transduction within cells to promote remyelination. More specifically, Mathews *et al.* showed that distinct signaling cascades downstream of Akt enhance myelin gene expression and axon myelination (85). Further, the authors demonstrate that cholesterol is necessary to promote mTOR kinase activity, which stimulates cholesterol synthesis (85). This way, RAM-derived EV-associated cholesterol might upregulate cholesterol synthesis in OPCs in a positive feedback loop. Altogether, more research is warranted to define how EV-derived cholesterol can promote OPC differentiation and remyelination.

Currently, there is no cure for MS. The available therapies reduce disease burden but are unable to stop neurologic decline as the disease advances (86). Therefore, there is an urgent need for novel therapies that are not only effective in the early inflammatory disease stage but also capable of inducing CNS repair in chronic disease stages. Given the pro-regenerative effect of RAM-derived EVs, our results open a window for a treatment based on EVs. In the past years, EV-based therapies have gained significant interest, as the therapeutic implications of EVs have several advantages over cell-based treatments. While cell-based therapies can often induce unwanted immunogenic responses, EVs are stable in biological solutions and have low immunogenicity (87). Currently, multiple clinical trials are ongoing to evaluate the application of EVs in several diseases, such as acute respiratory distress syndrome (ARDS; phase 1/2) and cancer (phase 1/2) (88-91). For example, a phase 1 study shows the feasible and safe immunization of stage III/IV metastatic melanoma patients with autologous DC-derived EVs. In this

clinical trial, EVs were isolated from DCs and loaded with MHC-I and MHC-II peptides, thereby promoting T cell immune responses and tumor rejection (90). Even during the global COVID-19 pandemic, EVs got the attention as a therapy for COVID-19-associated ARDS patients (92). More specifically, in a phase 2 clinical trial, bone marrow-derived mesenchymal stem cell-derived EVs were intravenously administered to patients with severe COVID-19 infection to alleviate inflammatory responses and restore the injured tissue. As promising results were obtained, the EV-based therapy will proceed to a phase 3 clinical trial (93), demonstrating the vast potential of EV-based treatments to treat various diseases. Furthermore, our results indicate that cholesterol plays a crucial role in promoting remyelination in the brain. As much research has already been performed on the beneficial effects of cholesterol on CNS repair, our results confirm the possibility of novel cholesterol-based therapies. For example, with the use of liposomes, which are spherical vesicles consisting of at least one lipid bilayer, cholesterol delivery to OPCs can be enhanced (94). However, further research is warranted to evaluate whether cholesterol-loaded liposomes can be a therapeutic approach of treating demyelinating diseases.

CONCLUSION

In summary, our findings indicate that RAMs promote OPC differentiation and remyelination through the release of EVs. The pro-regenerative impact of RAM-derived EVs was attributed to increased cholesterol levels present in these EVs. More research is needed to unravel the molecular mechanism that underlies the regenerative impact of EV-associated cholesterol. Taken together, our findings demonstrate that both EVs and cholesterol potentially have broad implications for therapeutic strategies aimed at promoting CNS repair.

REFERENCES

1. Hoftberger R, Lassmann H. Inflammatory demyelinating diseases of the central nervous system. Handb Clin Neurol. 2017;145:263-83.
2. Savransky A. [Demyelinating disorders]. Medicina (B Aires). 2018;78 Suppl 2:75-81.
3. Nylander A, Hafler DA. Multiple sclerosis. J Clin Invest. 2012;122(4):1180-8.
4. Azzopardi L, Thompson SA, Harding KE, Cossburn M, Robertson N, Compston A, et al. Predicting autoimmunity after alemtuzumab treatment of multiple sclerosis. J Neurol Neurosurg Psychiatry. 2014;85(7):795-8.
5. Zarini D, Pasbakhsh P, Nekoonam S, Mojaverrostami S, Ghasemi S, Shabani M, et al. Protective Features of Calorie Restriction on Cuprizone-induced Demyelination via Modulating Microglial Phenotype. J Chem Neuroanat. 2021;116:102013.
6. Ajami B, Bennett JL, Krieger C, McNagny KM, Rossi FM. Infiltrating monocytes trigger EAE progression, but do not contribute to the resident microglia pool. Nat Neurosci. 2011;14(9):1142-9.
7. Juhas U, Ryba-Stanislawowska M, Szargiej P, Mysliwska J. Different pathways of macrophage activation and polarization. Postepy Hig Med Dosw (Online). 2015;69:496-502.
8. Yamasaki R, Lu H, Butovsky O, Ohno N, Rietsch AM, Cialic R, et al. Differential roles of microglia and monocytes in the inflamed central nervous system. J Exp Med. 2014;211(8):1533-49.
9. Wynn TA, Vannella KM. Macrophages in Tissue Repair, Regeneration, and Fibrosis. Immunity. 2016;44(3):450-62.
10. Bogie JF, Stinissen P, Hendriks JJ. Macrophage subsets and microglia in multiple sclerosis. Acta Neuropathol. 2014;128(2):191-213.
11. Colonna M, Facchetti F. TREM-1 (triggering receptor expressed on myeloid cells): a new player in acute inflammatory responses. J Infect Dis. 2003;187 Suppl 2:S397-401.
12. Wang J, Wang J, Wang J, Yang B, Weng Q, He Q. Targeting Microglia and Macrophages: A Potential Treatment Strategy for Multiple Sclerosis. Front Pharmacol. 2019;10:286.
13. Grajchen E, Hendriks JJA, Bogie JFJ. The physiology of foamy phagocytes in multiple sclerosis. Acta Neuropathol Commun. 2018;6(1):124.
14. Franklin RJM, Ffrench-Constant C. Regenerating CNS myelin - from mechanisms to experimental medicines. Nat Rev Neurosci. 2017;18(12):753-69.
15. Baaklini CS, Rawji KS, Duncan GJ, Ho MFS, Plemel JR. Central Nervous System Remyelination: Roles of Glia and Innate Immune Cells. Front Mol Neurosci. 2019;12:225.
16. Fancy SP, Kotter MR, Harrington EP, Huang JK, Zhao C, Rowitch DH, et al. Overcoming remyelination failure in multiple sclerosis and other myelin disorders. Exp Neurol. 2010;225(1):18-23.

17. Wolswijk G. Oligodendrocyte precursor cells in the demyelinated multiple sclerosis spinal cord. Brain. 2002;125(Pt 2):338-49.
18. Hanafy KA, Sloane JA. Regulation of remyelination in multiple sclerosis. FEBS Lett. 2011;585(23):3821-8.
19. Hagemeier K, Bruck W, Kuhlmann T. Multiple sclerosis - remyelination failure as a cause of disease progression. Histol Histopathol. 2012;27(3):277-87.
20. Neumann B, Segel M, Chalut KJ, Franklin RJ. Remyelination and ageing: Reversing the ravages of time. Mult Scler. 2019;25(14):1835-41.
21. Wang F, Ren SY, Chen JF, Liu K, Li RX, Li ZF, et al. Myelin degeneration and diminished myelin renewal contribute to age-related deficits in memory. Nat Neurosci. 2020;23(4):481-6.
22. Woodruff RH, Fruttiger M, Richardson WD, Franklin RJ. Platelet-derived growth factor regulates oligodendrocyte progenitor numbers in adult CNS and their response following CNS demyelination. Mol Cell Neurosci. 2004;25(2):252-62.
23. Miron VE, Boyd A, Zhao JW, Yuen TJ, Ruckh JM, Shadrach JL, et al. M2 microglia and macrophages drive oligodendrocyte differentiation during CNS remyelination. Nat Neurosci. 2013;16(9):1211-8.
24. Lombardi M, Parolisi R, Scaroni F, Bonfanti E, Gualerzi A, Gabrielli M, et al. Detrimental and protective action of microglial extracellular vesicles on myelin lesions: astrocyte involvement in remyelination failure. Acta Neuropathol. 2019;138(6):987-1012.
25. Yanez-Mo M, Siljander PR, Andreu Z, Zavec AB, Borras FE, Buzas EI, et al. Biological properties of extracellular vesicles and their physiological functions. J Extracell Vesicles. 2015;4:27066.
26. Harding CV, Heuser JE, Stahl PD. Exosomes: looking back three decades and into the future. J Cell Biol. 2013;200(4):367-71.
27. Vanherle S, Haidar M, Irobi J, Bogie JFJ, Hendriks JJA. Extracellular vesicle-associated lipids in central nervous system disorders. Adv Drug Deliv Rev. 2020;159:322-31.
28. Bogie JF, Mailleux J, Wouters E, Jorissen W, Grajchen E, Vanmol J, et al. Scavenger receptor collectin placenta 1 is a novel receptor involved in the uptake of myelin by phagocytes. Sci Rep. 2017;7:44794.
29. Weischenfeldt J, Porse B. Bone Marrow-Derived Macrophages (BMM): Isolation and Applications. CSH Protoc. 2008;2008:pdb prot5080.
30. Tiane A, Schepers M, Riemens R, Rombaut B, Vandormael P, Somers V, et al. DNA methylation regulates the expression of the negative transcriptional regulators ID2 and ID4 during OPC differentiation. Cell Mol Life Sci. 2021;78(19-20):6631-44.
31. Bogie JFJ, Grajchen E, Wouters E, Corrales AG, Dierckx T, Vanherle S, et al. Stearoyl-CoA desaturase-1 impairs the reparative properties of macrophages and microglia in the brain. J Exp Med. 2020;217(5).
32. Meffre D, Massaad C, Grenier J. Lithium chloride stimulates PLP and MBP expression in oligodendrocytes via Wnt/beta-catenin and Akt/CREB pathways. Neuroscience. 2015;284:962-71.
33. Hussain R, El-Etr M, Gaci O, Rakotomamonjy J, Macklin WB, Kumar N, et al. Progesterone and Nestorone facilitate axon remyelination: a role for progesterone receptors. Endocrinology. 2011;152(10):3820-31.
34. Facchinetti R, Bronzuoli MR, Scuderi C. An Animal Model of Alzheimer Disease Based on the Intrahippocampal Injection of Amyloid beta-Peptide (1-42). Methods Mol Biol. 2018;1727:343-52.
35. Bogie J, Hoeks C, Schepers M, Tiane A, Cuypers A, Leijten F, et al. Dietary Sargassum fusiforme improves memory and reduces amyloid plaque load in an Alzheimer's disease mouse model. Sci Rep. 2019;9(1):4908.
36. Luga V, Zhang L, Viloria-Petit AM, Ogunjimi AA, Inanlou MR, Chiu E, et al. Exosomes mediate stromal mobilization of autocrine Wnt-PCP signaling in breast cancer cell migration. Cell. 2012;151(7):1542-56.
37. Zomer A, Maynard C, Verweij FJ, Kamermans A, Schafer R, Beerling E, et al. In Vivo imaging reveals extracellular vesicle-mediated phenocopying of metastatic behavior. Cell. 2015;161(5):1046-57.
38. Mitchell R, Mellows B, Sheard J, Antonioli M, Kretz O, Chambers D, et al. Secretome of adipose-derived mesenchymal stem cells promotes skeletal muscle regeneration through synergistic action of extracellular vesicle cargo and soluble proteins. Stem Cell Res Ther. 2019;10(1):116.

39. Thery C, Witwer KW, Aikawa E, Alcaraz MJ, Anderson JD, Andriantsitohaina R, et al. Minimal information for studies of extracellular vesicles 2018 (MISEV2018): a position statement of the International Society for Extracellular Vesicles and update of the MISEV2014 guidelines. J Extracell Vesicles. 2018;7(1):1535750.
40. Hubler Z, Allimuthu D, Bederman I, Elitt MS, Madhavan M, Allan KC, et al. Accumulation of 8,9-unsaturated sterols drives oligodendrocyte formation and remyelination. Nature. 2018;560(7718):372-6.
41. Dimas P, Montani L, Pereira JA, Moreno D, Trotzmuller M, Gerber J, et al. CNS myelination and remyelination depend on fatty acid synthesis by oligodendrocytes. Elife. 2019;8.
42. Saher G, Brugger B, Lappe-Siefke C, Mobius W, Tozawa R, Wehr MC, et al. High cholesterol level is essential for myelin membrane growth. Nat Neurosci. 2005;8(4):468-75.
43. Tabas I. Consequences of cellular cholesterol accumulation: basic concepts and physiological implications. J Clin Invest. 2002;110(7):905-11.
44. Berghoff SA, Gerndt N, Winchenbach J, Stumpf SK, Hosang L, Odoardi F, et al. Dietary cholesterol promotes repair of demyelinated lesions in the adult brain. Nat Commun. 2017;8:14241.
45. Berghoff SA, Spieth L, Sun T, Hosang L, Depp C, Sasmita AO, et al. Neuronal cholesterol synthesis is essential for repair of chronically demyelinated lesions in mice. Cell Rep. 2021;37(4):109889.
46. Voskuhl RR, Itoh N, Tassoni A, Matsukawa MA, Ren E, Tse V, et al. Gene expression in oligodendrocytes during remyelination reveals cholesterol homeostasis as a therapeutic target in multiple sclerosis. Proc Natl Acad Sci U S A. 2019;116(20):10130-9.
47. Berghoff SA, Spieth L, Saher G. Local cholesterol metabolism orchestrates remyelination. Trends Neurosci. 2022;45(4):272-83.
48. Chari DM. Remyelination in multiple sclerosis. Int Rev Neurobiol. 2007;79:589-620.
49. Hess K, Starost L, Kieran NW, Thomas C, Vincenten MCJ, Antel J, et al. Lesion stage-dependent causes for impaired remyelination in MS. Acta Neuropathol. 2020;140(3):359-75.
50. Franklin RJ, Ffrench-Constant C. Remyelination in the CNS: from biology to therapy. Nat Rev Neurosci. 2008;9(11):839-55.
51. Keough MB, Yong VW. Remyelination therapy for multiple sclerosis. Neurotherapeutics. 2013;10(1):44-54.
52. Kotter MR, Stadelmann C, Hartung HP. Enhancing remyelination in disease--can we wrap it up? Brain. 2011;134(Pt 7):1882-900.
53. Kotter MR, Zhao C, van Rooijen N, Franklin RJ. Macrophage-depletion induced impairment of experimental CNS remyelination is associated with a reduced oligodendrocyte progenitor cell response and altered growth factor expression. Neurobiol Dis. 2005;18(1):166-75.
54. Butovsky O, Landa G, Kunis G, Ziv Y, Avidan H, Greenberg N, et al. Induction and blockage of oligodendrogenesis by differently activated microglia in an animal model of multiple sclerosis. J Clin Invest. 2006;116(4):905-15.
55. Tian J, Casella G, Zhang Y, Rostami A, Li X. Potential roles of extracellular vesicles in the pathophysiology, diagnosis, and treatment of autoimmune diseases. Int J Biol Sci. 2020;16(4):620-32.
56. Minciacchi VR, Spinelli C, Reis-Sobreiro M, Cavallini L, You S, Zandian M, et al. MYC Mediates Large Oncosome-Induced Fibroblast Reprogramming in Prostate Cancer. Cancer Res. 2017;77(9):2306-17.
57. Zitvogel L, Regnault A, Lozier A, Wolfers J, Flament C, Tenza D, et al. Eradication of established murine tumors using a novel cell-free vaccine: dendritic cell-derived exosomes. Nat Med. 1998;4(5):594-600.
58. Lopez P, Rodriguez-Carrio J, Caminal-Montero L, Suarez A. Relationship Between T-Cell Exosomes and Cellular Subsets in SLE According to Type I IFN-Signaling. Front Med (Lausanne). 2020;7:604098.
59. Acquatella-Tran Van Ba I, Imberdis T, Perrier V. From prion diseases to prion-like propagation mechanisms of neurodegenerative diseases. Int J Cell Biol. 2013;2013:975832.
60. Fevrier B, Vilette D, Archer F, Loew D, Faigle W, Vidal M, et al. Cells release prions in association with exosomes. Proc Natl Acad Sci U S A. 2004;101(26):9683-8.
61. Poitelon Y, Kopec AM, Belin S. Myelin Fat Facts: An Overview of Lipids and Fatty Acid Metabolism. Cells. 2020;9(4).
62. Skotland T, Sagini K, Sandvig K, Llorente A. An emerging focus on lipids in extracellular vesicles. Adv Drug Deliv Rev. 2020;159:308-21.

63. Hough KP, Wilson LS, Trevor JL, Strenkowski JG, Maina N, Kim YI, et al. Unique Lipid Signatures of Extracellular Vesicles from the Airways of Asthmatics. Sci Rep. 2018;8(1):10340.
64. Nishida-Aoki N, Izumi Y, Takeda H, Takahashi M, Ochiya T, Bamba T. Lipidomic Analysis of Cells and Extracellular Vesicles from High- and Low-Metastatic Triple-Negative Breast Cancer. Metabolites. 2020;10(2).
65. Haraszti RA, Didiot MC, Sapp E, Leszyk J, Shaffer SA, Rockwell HE, et al. High-resolution proteomic and lipidomic analysis of exosomes and microvesicles from different cell sources. J Extracell Vesicles. 2016;5:32570.
66. Bruce KD, Zsombok A, Eckel RH. Lipid Processing in the Brain: A Key Regulator of Systemic Metabolism. Front Endocrinol (Lausanne). 2017;8:60.
67. Barber CN, Raben DM. Lipid Metabolism Crosstalk in the Brain: Glia and Neurons. Front Cell Neurosci. 2019;13:212.
68. Grey M, Dunning CJ, Gaspar R, Grey C, Brundin P, Sparr E, et al. Acceleration of alpha-synuclein aggregation by exosomes. J Biol Chem. 2015;290(5):2969-82.
69. Su H, Rustam YH, Masters CL, Makalic E, McLean CA, Hill AF, et al. Characterization of brain-derived extracellular vesicle lipids in Alzheimer's disease. J Extracell Vesicles. 2021;10(7):e12089.
70. Moyano AL, Li G, Boullerne AI, Feinstein DL, Hartman E, Skias D, et al. Sulfatides in extracellular vesicles isolated from plasma of multiple sclerosis patients. J Neurosci Res. 2016;94(12):1579-87.
71. Lorincz B, Jury EC, Vrablik M, Ramanathan M, Uher T. The role of cholesterol metabolism in multiple sclerosis: From molecular pathophysiology to radiological and clinical disease activity. Autoimmun Rev. 2022;21(6):103088.
72. Martin MG, Pfrieger F, Dotti CG. Cholesterol in brain disease: sometimes determinant and frequently implicated. EMBO Rep. 2014;15(10):1036-52.
73. Casella G, Colombo F, Finardi A, Descamps H, Ill-Raga G, Spinelli A, et al. Extracellular Vesicles Containing IL-4 Modulate Neuroinflammation in a Mouse Model of Multiple Sclerosis. Mol Ther. 2018;26(9):2107-18.
74. Mahammad S, Parmryd I. Cholesterol depletion using methyl-beta-cyclodextrin. Methods Mol Biol. 2015;1232:91-102.
75. Nishijo J, Moriyama S, Shiota S. Interactions of cholesterol with cyclodextrins in aqueous solution. Chem Pharm Bull (Tokyo). 2003;51(11):1253-7.
76. Zidovetzki R, Levitan I. Use of cyclodextrins to manipulate plasma membrane cholesterol content: evidence, misconceptions and control strategies. Biochim Biophys Acta. 2007;1768(6):1311-24.
77. Venkateswaran A, Laffitte BA, Joseph SB, Mak PA, Wilpitz DC, Edwards PA, et al. Control of cellular cholesterol efflux by the nuclear oxysterol receptor LXR alpha. Proc Natl Acad Sci U S A. 2000;97(22):12097-102.
78. Kennedy MA, Venkateswaran A, Tarr PT, Xenarios I, Kudoh J, Shimizu N, et al. Characterization of the human ABCG1 gene: liver X receptor activates an internal promoter that produces a novel transcript encoding an alternative form of the protein. J Biol Chem. 2001;276(42):39438-47.
79. Chen W, Chen G, Head DL, Mangelsdorf DJ, Russell DW. Enzymatic reduction of oxysterols impairs LXR signaling in cultured cells and the livers of mice. Cell Metab. 2007;5(1):73-9.
80. Yang C, McDonald JG, Patel A, Zhang Y, Umetani M, Xu F, et al. Sterol intermediates from cholesterol biosynthetic pathway as liver X receptor ligands. J Biol Chem. 2006;281(38):27816-26.
81. Nelissen K, Mulder M, Smets I, Timmermans S, Smeets K, Ameloot M, et al. Liver X receptors regulate cholesterol homeostasis in oligodendrocytes. J Neurosci Res. 2012;90(1):60-71.
82. Xu P, Xu H, Tang X, Xu L, Wang Y, Guo L, et al. Liver X receptor beta is essential for the differentiation of radial glial cells to oligodendrocytes in the dorsal cortex. Mol Psychiatry. 2014;19(8):947-57.
83. Meffre D, Shackleford G, Hichor M, Gorgievski V, Tzavara ET, Trousson A, et al. Liver X receptors alpha and beta promote myelination and remyelination in the cerebellum. Proc Natl Acad Sci U S A. 2015;112(24):7587-92.
84. Mulcahy LA, Pink RC, Carter DR. Routes and mechanisms of extracellular vesicle uptake. J Extracell Vesicles. 2014;3.

85. Mathews ES, Appel B. Cholesterol Biosynthesis Supports Myelin Gene Expression and Axon Ensheathment through Modulation of P13K/Akt/mTor Signaling. J Neurosci. 2016;36(29):7628-39.
86. Kremer D, Akkermann R, Kury P, Dutta R. Current advancements in promoting remyelination in multiple sclerosis. Mult Scler. 2019;25(1):7-14.
87. Zhu X, Badawi M, Pomeroy S, Sutaria DS, Xie Z, Baek A, et al. Comprehensive toxicity and immunogenicity studies reveal minimal effects in mice following sustained dosing of extracellular vesicles derived from HEK293T cells. J Extracell Vesicles. 2017;6(1):1324730.
88. Dai S, Wei D, Wu Z, Zhou X, Wei X, Huang H, et al. Phase I clinical trial of autologous ascites-derived exosomes combined with GM-CSF for colorectal cancer. Mol Ther. 2008;16(4):782-90.
89. Morse MA, Garst J, Osada T, Khan S, Hobeika A, Clay TM, et al. A phase I study of dexosome immunotherapy in patients with advanced non-small cell lung cancer. J Transl Med. 2005;3(1):9.
90. Escudier B, Dorval T, Chaput N, Andre F, Caby MP, Novault S, et al. Vaccination of metastatic melanoma patients with autologous dendritic cell (DC) derived-exosomes: results of thefirst phase I clinical trial. J Transl Med. 2005;3(1):10.
91. Grangier A, Branchu J, Volatron J, Piffoux M, Gazeau F, Wilhelm C, et al. Technological advances towards extracellular vesicles mass production. Adv Drug Deliv Rev. 2021;176:113843.
92. Karn V, Ahmed S, Tsai LW, Dubey R, Ojha S, Singh HN, et al. Extracellular Vesicle-Based Therapy for COVID-19: Promises, Challenges and Future Prospects. Biomedicines. 2021;9(10).
93. Sengupta V, Sengupta S, Lazo A, Woods P, Nolan A, Bremer N. Exosomes Derived from Bone Marrow Mesenchymal Stem Cells as Treatment for Severe COVID-19. Stem Cells Dev. 2020;29(12):747-54.
94. Nisini R, Poerio N, Mariotti S, De Santis F, Fraziano M. The Multirole of Liposomes in Therapy and Prevention of Infectious Diseases. Front Immunol. 2018;9:155.

Acknowledgements – Jeroen Guns expresses his sincere gratitude to his supervisor Sam Vanherle and promoter Prof. dr. Jeroen Bogie for their consistent support, scientific and practical opportunities, and guidance throughout the process of his senior internship and writing this paper. Jeroen Guns would also like to thank the members of the "Immunology and Infection" group for their support throughout his internship. This work was financially supported by the Research Foundation of Flanders (FWO Vlaanderen; 1S15519N, G099618FWO and 12J9119N).

Author contributions – Prof. dr. Jeroen Bogie and Sam Vanherle conceived and designed the experiments. Jeroen Guns and Sam Vanherle performed experiments and data analysis. Jeroen Guns wrote the paper. All authors carefully edited the manuscript.

SUPPLEMENTARY EXPERIMENTAL PROCEDURES (SEP)

Nanoparticle Tracking Analysis – To determine the size and concentration of BMDM-derived EVs with different phenotypes, Nanoparticle Tracking Analysis (NTA) was performed using the NanoSight NS 300 system (Malvern Panalytical), equipped with a 532 nm laser. Samples were diluted in 1x PBS over a concentration range between 20 and 50 particles per frame. All settings were manually set at the beginning of the measurements and kept constant during all acquisitions: camera level 14, camera gain 1, pump rate 80, viscosity 1. A minimum of three recordings of 60 s were recorded and analyzed using the NTA software 3.0 with default settings.

Western blot – EVs were lysed on ice for 30 min in ice-cold RIPA buffer (ThermoFisher Scientific) and pelleted at 17,000 g at 4°C for 15 min. Protein concentrations were determined using the Pierce BCA protein assay kit (ThermoFisher Scientific) according to the manufacturer's protocol and by using the CLARIOstar PLUS microplate reader (BMG Labtech). Proteins were denatured using a 5X sample buffer followed by heating the sample at 95°C for 5 min. Afterwards, the samples were loaded on a 12% SDS-PAGE gel and transferred to the polyvinylidene difluoride blotting membrane (Merck). Blocking was performed using 5% dried skimmed milk powder (Marvel) in 1X PBS-0.1% Tween-20 (PBS-T). The blotting membranes were incubated overnight with specific primary antibodies at 4°C. The next day, horseradish peroxidase conjugated (HRP) secondary antibodies (Dako), at a dilution of 1/2000, were added to the blotting membrane for 1 h at room temperature. WesternBright Sirius HRP substrate (Advansta) was used to generate chemiluminescent signals which were detected with the Amersham Imager 680 (GE Healthcare Life Sciences). Primary antibodies used: Flotillin 1 (1:1,000; ab232405; Abcam), CD81 (1:1,000; ab109201; Abcam), Annexin A2 (1:1,000; ab178677; Abcam), GRP94 (1:1,000; ab238126; Abcam).

LC-ESI-MS/MS – LPS- and IL-4-stimulated BMDM-derived EV pellets were diluted in 700 µl 1x PBS with 800 µl 1 N HCl:CH3OH 1:8 (v/v), 900 µl ChCl3 and 200 µg/ml of the antioxidant 2,6-di-tert-butyl-4-methylphenol (BHT; Sigma-Aldrich). 3 µl of SPLASH LIPIDOMIX Mass Spec Standard (Avanti Polar Lipids) was added into the extract mix. The organic fraction was evaporated at room temperature using the Savant Speedvac spd111v (ThermoFisher Scientific), and the remaining lipid pellet was reconstituted in 100% ethanol. Lipid species were analyzed by liquid chromatography-electrospray ionization tandem mass spectrometry (LC-ESI-MS/MS) on a Nexera X2 UHPLC system (Shimadzu) coupled with hybrid triple quadrupole/linear ion trap mass spectrometer (6500+ QTRAP system; AB SCIEX). Chromatographic separation was performed on a XBridge amide column (150 mm x 4.6 mm, 3x5 µm; Waters) maintained at 35°C using mobile phase A [1 mM ammonium acetate in water-acetonitrile 5:95 (v/v)] and mobile phase B [1 mM ammonium acetate in water-acetonitrile 50:50 (v/v)] in the following gradient: (0-6 min: 0% B → 6% B; 6-10 min: 6% B → 25% B; 10-11 min: 25% B → 98% B; 11-13 min: 98% B → 100% B; 13-19 min: 100% B; 19-24 min: 0% B) at a flow rate of 0.7 ml/min which was increased to 1.5 ml/min from 13 minutes onwards. Sphingomyelin (SM) and cholesteryl esters (CE) were measured in positive ion mode with a precursor scan of 184.1, 369.4. Triglycerides (TG) were measured in positive ion mode with a neutral loss scan for one of the fatty acyl moieties. Phosphatidylcholines (PC) and phosphatidylserines (PS) were measured in negative ion mode by fatty acyl fragment ions. Lipid quantification was performed by scheduled multiple reactions monitoring, the transitions being based on the neutral losses or the typical product ions as described above. The instrument parameters were as follows: Curtain Gas = 35 psi; Collision Gas = 8 a.u. (medium); IonSpray Voltage = 5500 V and -4500 V; Temperature = 550 °C; Ion Source Gas 1 = 50 psi; Ion Source Gas 2 = 60 psi; Declustering Potential = 60 V and -80 V; Entrance Potential = 10 V and -10 V; Collision Cell Exit Potential = 15 V and -15 V. Peak integration was performed with the Multiquant TM software version 3.0.3. Lipid species signals were corrected for isotopic contributions (calculated with Python Molmass 2019.1.1) and were quantified based on internal standard signals and adhere to the guidelines of the Lipidomics Standards Initiative. Only the most prevalent lipid classes present in EVs are reported.

SUPPLEMENTARY FIGURES

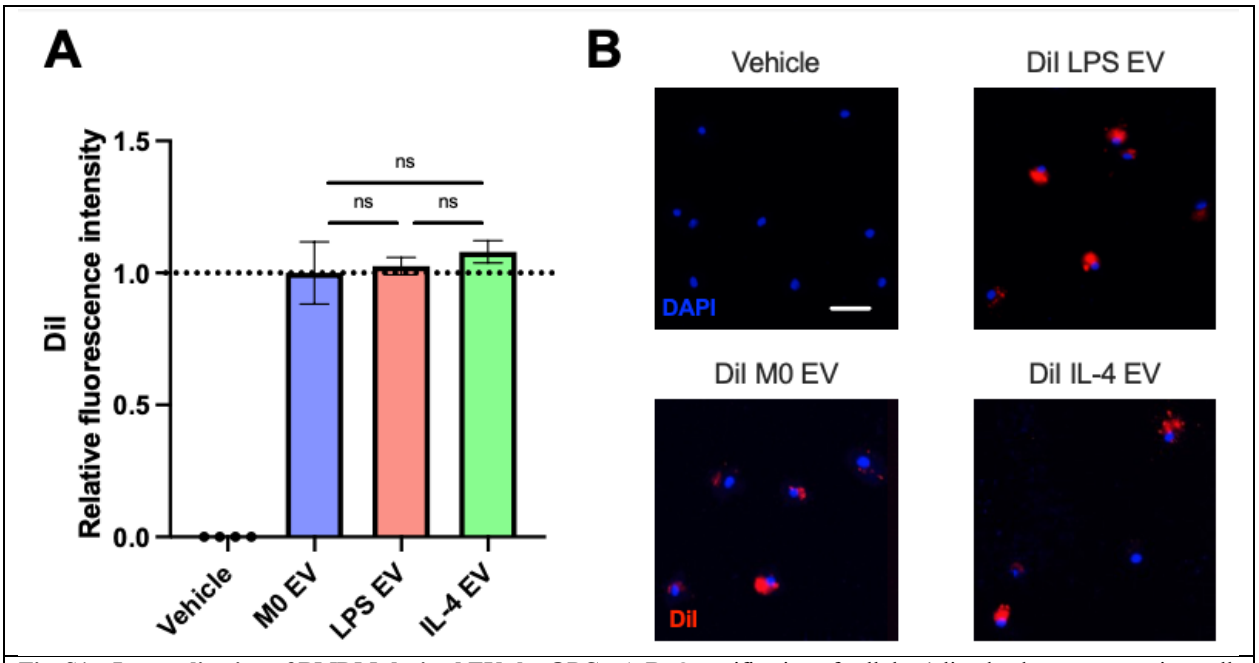

Fig. S1 – **Internalization of BMDM-derived EVs by OPCs**. **A-B**: Quantification of cellular (oligodendrocyte progenitor cell; OPC) uptake of DiI-labeled extracellular vesicles (EVs) derived from naive (M0 EV), LPS-stimulated (LPS EV), IL-4-stimulated (IL-4 EV) bone marrow-derived macrophages by means of flow cytometry (A) and immunocytochemistry (B) (n = 4 biological replicates; scale bar, 5 µm). All data are represented as mean ± SEM. ****, P < 0.0001; one-way ANOVA.

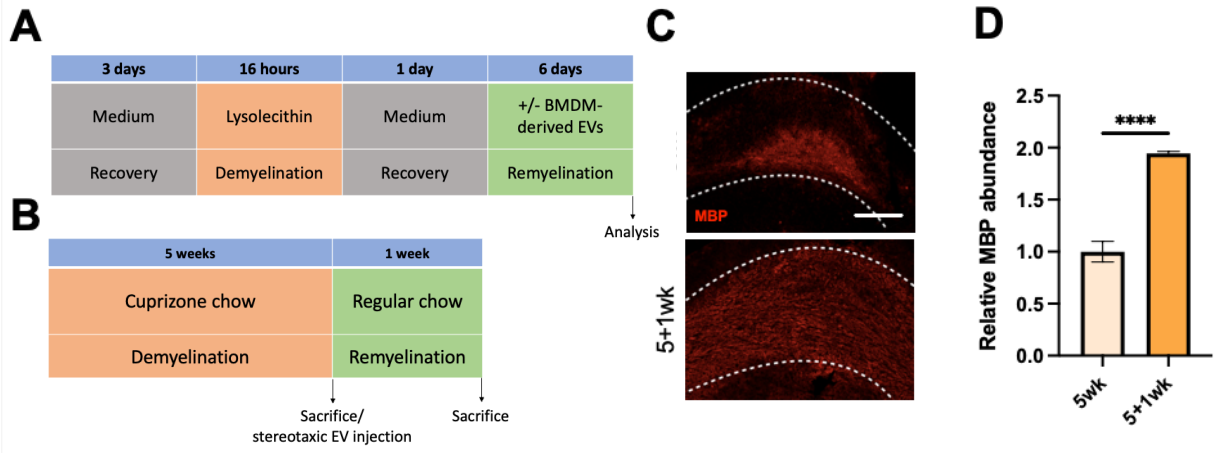

Fig. S2 – ***Ex vivo* and *in vivo* experimental setup**. **A-B**: Experimental setup of the *ex vivo* cerebellar brain slice model (A) and the cuprizone-induced acute demyelination *in vivo* model (B). **C-D**: Representative images of immunofluorescence MBP staining (C) of the corpus callosum (CC) from mice analyzed (D) after five weeks of cuprizone-induced demyelination (5wk) or stereotaxically injected with vehicle (PBS) and analyzed after one week of subsequent remyelination (5+1wk). The outer border of the CC is lined with a dotted line (scale bar, 150 µm). All data are represented as mean ± SEM. ****, P < 0.0001; Student's t-test.

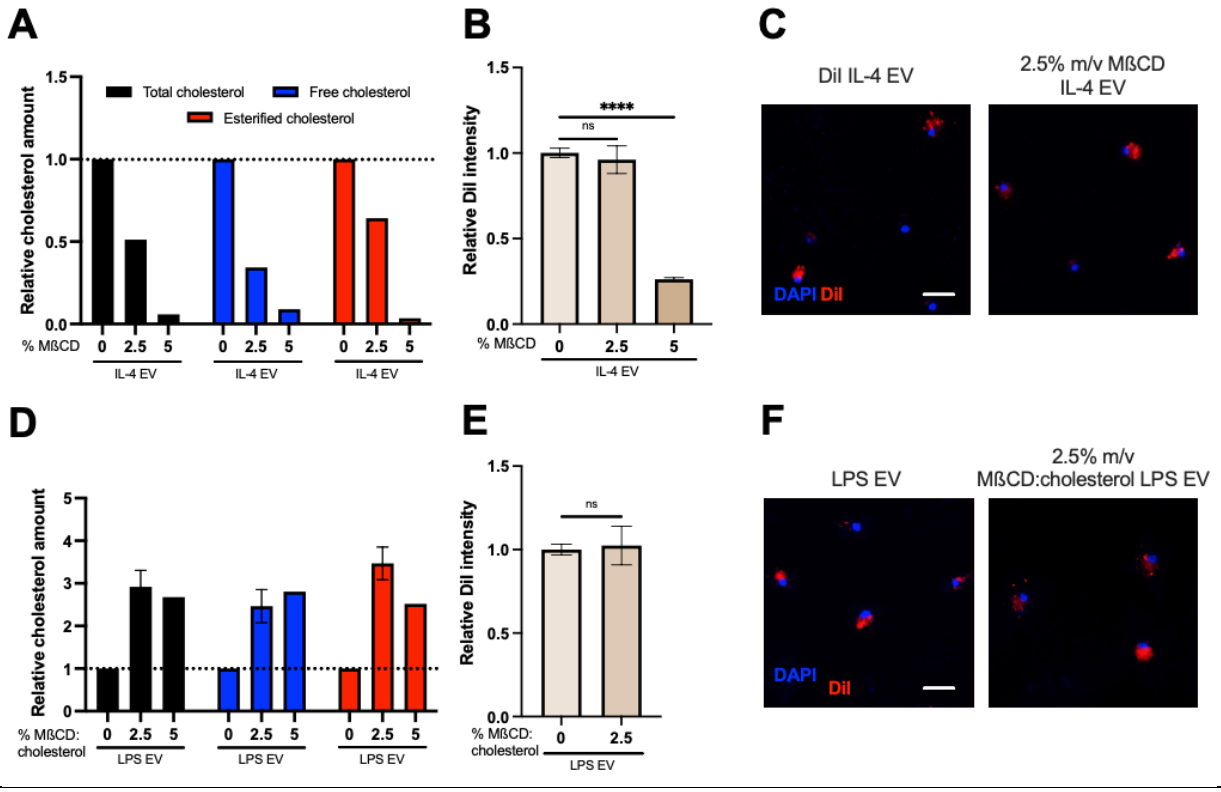

Fig. S3 – **Cholesterol depletion and repletion of EVs secreted by RAMs and DAMS, respectively**. **A-C**: Cholesterol depletion of extracellular vesicles (EVs) derived from IL-4-stimulated (IL-4 EV) bone marrow-derived macrophages (BMDMs). Quantification of total cholesterol, free cholesterol, and cholesterol esters (A) in IL-4 EVs incubated with 0 (dotted line), 2.5, or 5% m/v methyl-ß-cyclodextrin (MßCD) for 1 h at 37°C (n = 1 biological replicate). Quantification of cellular uptake of oligodendrocyte progenitor cells (OPCs) exposed for 3 h to 0, 2.5, or 5% m/v MßCD-treated DiI-labeled IL-4 EV by means of flow cytometry (B) and immunocytochemistry (C) (5% m/v MßCD IL-4 EV not shown) (n = 4 biological replicates; scale bar, 5 µm). **D-F**: Cholesterol replenishment of extracellular vesicles (EVs) derived from LPS-stimulated (LPS EV) BMDMs. Quantification of total cholesterol, free cholesterol, and cholesterol esters (D) in LPS EVs incubated with 0 (dotted line), 2.5, or 5% m/v MßCD:cholesterol mixture (MßCD:cholesterol) overnight while shaking at 37°C (n = 1-2 biological replicate(s)). Quantification of cellular uptake of OPCs exposed for 3 h to 0 or 2.5 m/v MßCD:cholesterol-treated DiI-labeled LPS EV by means of flow cytometry (E) and immunocytochemistry (F) (n = 4 biological replicates; scale bar, 5 µm). All data are represented as mean ± SEM. Non-significant (ns), $P > 0.05$; ****, $P < 0.0001$; one-way ANOVA (B), Student's t-test (E).

Suppl. Table 1 – **List of antibodies used for immunofluorescence**.

Antigen	Company (reference number)	Dilution
MBP (*in vitro* and *in vivo*)	Millipore (MAB386)	1:500 (*in vitro*) 1:250 (*in vivo*)
O4	R&D systems (MAB1326)	1:1,000
MBP (*ex vivo*)	Bio-Rad (MCA409S)	1:250
NF	Abcam (ab8135)	1:1,000
Olig2	R&D systems (AF2418)	1:50
CC1	Abcam (ab16794)	1:50
DiI	Sigma-Aldrich	1:100
DAPI	Sigma-Aldrich	1:10,000

Goat anti-rat IgG	Invitrogen (A21434)	1:600 (*in vitro*) 1:400 (*ex vivo*) 1:500 (*in vivo*)
Goat anti-mouse IgM	Invitrogen (A21042)	1:600
Goat anti-rabbit IgG	Invitrogen (A11008)	1:500
Donkey anti-goat IgG	Invitrogen (A11055)	1:400
Donkey anti-mouse IgG	Invitrogen (A31570)	1:400